UNIVERSITÀ DEGLI STUDI DELL'INSUBRIA

Facoltà di Scienze Matematiche, Fisiche e Naturali

Dipartimento di Fisica e Matematica

Dottorato di Ricerca in Astronomia e Astrofisica

BLAZARS AS ASTROPHYSICAL AND COSMOLOGICAL PROBES

Supervisor:

Prof. Francesco Haardt

Massimo Cavadini

Matricola 610606

XXIV Ciclo

Contents

Preface

In the last three years the number of extragalactic γ-ray sources increased dramatically thanks to *AGILE* and *Fermi* γ-ray telescopes and to new improvements in the ground based Cherenkov detectors. Blazars, radio loud Active Galactic Nuclei (AGN) with a relativistic jet pointing toward the Earth, result to be the most common sources in the extragalactic γ-ray sky. In the GeV band up to one thousand sources have been detected in the extragalactic sky, allowing statistical studies of blazar sources.

γ-ray astrophysics has significant connections with other apparently far and different branches of astrophysics and cosmology. γ-ray photons are absorbed by lower energy optical and infrared radiation as they travel toward the Earth. The study of the absorbed spectra of blazars allows to put constraints on the intergalactic magnetic field (IGMF), on the intensity of Extragalactic Background Light and also on the cross section and mass of annihilating dark matter (DM) particles. During my PhD I have computed the contribution of blazars to the Extragalactic γ-ray Background (EGB) and I have derived an upper limit on the role played by annihilating DM. Moreover studying the cascade generated by the absorption of γ-ray photons by EBL I have derived new lower limits on the IGMF intensity. Finally I have proposed a new theoretical model for the EBL.

Chapter 1

Introduction

1.1 Status of the VHE astrophysics

The term γ-ray astrophysics is applied to photons that span 14 orders of magnitude, between 0.5×10^6 eV to $\sim 10^{20}$ eV. The lower bound is due to the electron/positron pair annihilation while the upper bound characterizes the energy of photons produced by the highest energy particle observed in cosmic rays. γ-ray astrophysics is divided in six areas: *low* (LE: below 30 MeV), *high* (HE: 30 MeV-30 GeV), *very high* (VHE: 30 GeV-30 TeV), *ultra high* (UHE: 30 TeV-30 PeV) and finally extremely high (EHE: above 30 PeV) energies. In this thesis we refer only to VHE γ-ray astrophysics. In this range of energies, observations are performed by orbiting telescopes (30 MeV-100 GeV) and by ground based detectors (100 GeV-20 TeV). In the following sections we review briefly the features of these two classes of detectors and their evolution. Accurate review articles can be found in Aharonian & Volk (2001), Enomoto et al. (2003) and Aharonian (2004).

1.2 γ-ray space telescopes

The γ-ray satellites are based on the conversion of the primary photons to an electron-positron pairs and on the subsequent measurements of the tracks

of the secondary electrons with tracking detectors and their energy with a total-absorption calorimeter. This technique allows the reconstruction of the arrival direction and energy of the primary γ-rays. The energy resolution is mainly due to the absorbing capability of the calorimeter.

The first significant γ-ray observational results appeared in the 70s due to the satellites *SAS-2* (Fichtel, Simpson, & Thompson 1978) and *COS B* (e.g. Bignami & Hermsen 1983). *SAS-2* detected four point sources while *COS-B* mission increased the number of sources to 25 one of which was identified with the quasar 3C 273 that was the first extragalactic γ-ray sources detected.

The *EGRET*, as part of the Compton Gamma Ray Observatory mission, during nine years of operations (1991-2000) detected 271 sources of which 66 extragalactic (Hartman et al. 1999). The large majority of these extragalactic sources were blazars. Moreover the telescope has provided the first reliable measure of the Extragalactic γ-ray background (EGB) in the 20 MeV-30 GeV band (Strong, Moskalenko, & Reimer 2004).

On 2008 June 11 the Gamma-ray Large Area Space Telescope (GLAST) was launched to improve the previous *EGRET* observations. Shortly after entering its scientific operating mission, on 2008 August, GLAST was renamed *Fermi* Gamma-ray Space Telescope. The main instrument onboard *Fermi* is the Large Area Telescope (LAT), a pair conversion telescope covering the energy band from 20 MeV up to 300 GeV (e.g. Atwood et al. 2009). In the sky-survey mode, LAT observes the entire sky every 3 hours.

After three years of observations (September 2011) *Fermi*-LAT has detected 861 extragalactic sources with high confidence allowing a statistical study of extragalactic γ-ray sources and providing a strong improvement in the EGB (see section 2.2.4 for further details and Fig. 1.1). Fig. 1.2 shows the comparison between the diffuse component of EGB detected by *EGRET* and by *Fermi*.

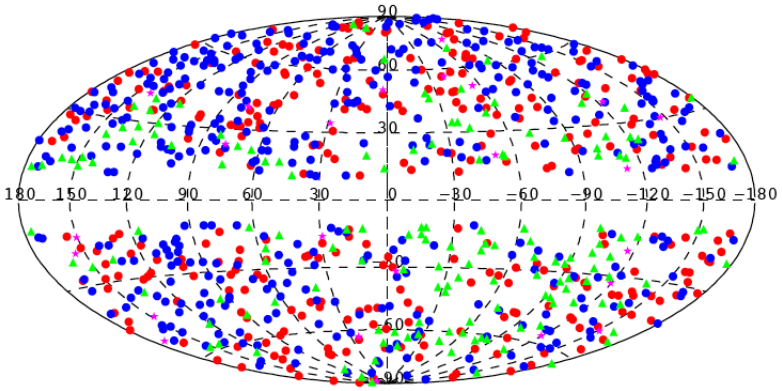

Figure 1.1: Locations of the sources in the Clean Sample of the 2LAC (see chapter 2). Red: FSRQs, blue: BL Lacs, magenta: non-blazar AGNs, green: AGNs of unknown type (from The *Fermi* collaboration 2011).

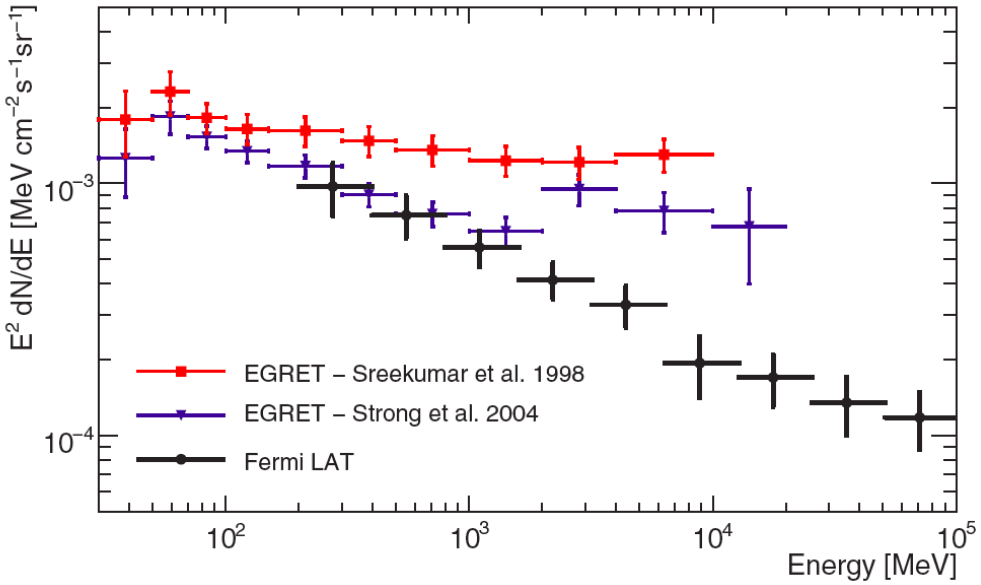

Figure 1.2: The comparison between the *EGRET* and *Fermi*-LAT γ-ray diffuse emission (from Abdo et al. 2010a)

1.3 Ground based detectors

At higher energies, above 100 GeV, satellite-based detectors are not efficient because of the low fluxes involved. Ground based detectors represent the best way to measure γ-ray photons in the upper VHE band. It is well known that VHE γ-ray are absorbed by the Earth atmosphere and produce extended atmospheric showers of hadron particle. Thus array of particle (muon, electron, hadron) detectors used in the traditional cosmic rays experiments were first been used as tools to indirectly detect γ-rays photons on Earth. The first experiment built with this aim was CASA-MIA (Borione et al. 1994). Imaging Atmospheric Cherenkov Telescopes (IACTs) use a more efficient technique. They detect the Cherenkov light produced by particles in atmosphere generated by γ-ray photons using an optical telescope that focus the Cherenkov light of a shower into a pixelized camera. The four major IACT experiments at are MAGIC (Colin et al. 2009), HESS (Chaves 2009), CANGAROO III (Kushida et al. 2003) and VERITAS (Holder 2007). These four collaborations are involved in the ambitious project called Cherenkov Telescope Array (CTA). The idea is to build an array of IACTs with a lower threshold and a better sensitivity. Up to now (September 2011) 46 extragalactic sources have been detected by IACTs above 300 GeV, (Fig. 1.3) of which the large majority are BL-Lacs.

Fig. 1.4 shows the so-called Kifune plot in which the evolution of source detection is displayed.

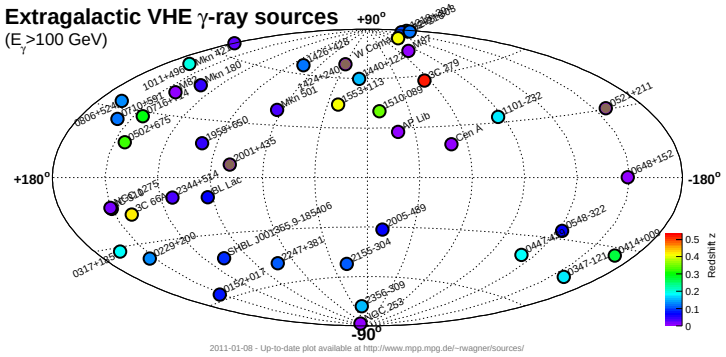

Figure 1.3: The VHE (>300 GeV) maps for extragalactic sourced detected by IACTs (From http://www.mpp.mpg.de/ rwagner/sources/)

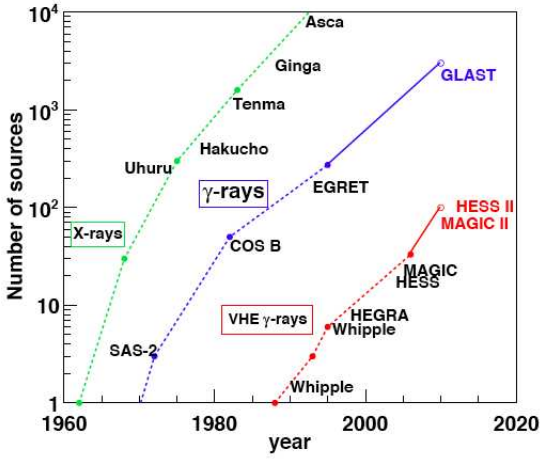

Figure 1.4: The Kifune plot: the number of source as function of time for X-ray (green line), γ-ray (blue line) and very high energy γ-ray (red-line) (From Mazin 2007).

Chapter 2

Extragalactic γ-ray background

2.1 Introduction

The EGB represents a fascinating challenge since his first detection by *SAS 2* satellite above 30 MeV (Fichtel, Simpson, & Thomson 1978). The γ-ray telescope *EGRET*, improving the *SAS 2* detection, measure a isotropic γ-ray emission in the 30 MeV-30 GeV range. The spectrum of the diffuse EGB component, that is the emission due to unresolved sources and/or truly diffuse processes, can be fit over the entire band with a power law with photon spectral index $\Gamma \sim 2.1 \pm 0.03$ (Sreekumar et al. 1998; Strong Moskalenko and Reimer 2004). This value is similar to the average photon index of blazars detected by *EGRET*. This result and the fact that blazars are the most common objects in the γ-ray sky, led the community to propose models able to explain the EGB shape in terms of blazar emission (Padovani et al. 1993; Stecker Salamon & Malkan 1993; Chiang et al. 1995; Stecker & Salamon 1996; Mucke & Powl 2000; Dermer et al. 2007; Inoue & Totani 2009, Stecker & Venters 2010; Venters & Pavlidou 2011)

As the new EGB measure performed by *Fermi*-LAT is more steeper and with a lower intensity than the *EGRET* EGB (see section 2.3), different theoretical models have been proposed. In particular the emission coming from star-forming galaxies should explain from a large fraction up to the totality

of the EGB (e.g. Dermer 2007 for a review).

Other components invoked to account for the EGB are clusters of galaxies (Berezinsky, Blasi & Ptuskin 1997), Gamma ray Bursts (Dermer 2007) and Pulsars (Faucher-Giguere & Loeb 2010). Truly diffuse component could be produced by the electromagnetic cascades due to the interaction between γ-ray photons from blazars and the EBL generated by galaxies over the cosmic history (Coppi and Aharonian 1997; see chapter 3 for further details). Also Ultra High Cosmic Rays interacting with the CMB generate a pair cascade which emits photon in the γ-ray band (e.g. Berezinsky et al. 2011). To the EGB can also contribute exotic diffuse sources as decaying or annihilating Dark Matter (DM) (see the section 2.7).

In this chapter we show the contribution of blazars (either FSRQs and BL-Lacs) to the *Fermi*-LAT EGB. To fully account for the total EGB star-forming galaxy component is needed. We add this component to our blazar model and fitting the *Fermi*-LAT EGB we put an upper limit on the mass of annihilating DM particles.

In the section 2.2 a review of blazars, their features and their emission mechanisms is proposed while the features of the EGB measured by *Fermi* is shown in the section 2.3. Then we will show the contribution of blazar (section 2.4), the results obtained (section 2.5), the star-forming galaxies (section 2.6) and the DM (section 2.7) component . Discussion and conclusions are shown in section 2.8.

2.2 Blazars

2.2.1 General features

It is well established that galaxies host in their center a supermassive (from 3×10^6 to 3×10^9 $M_\odot$) black hole (hereafter SMBH) whose mass correlates with the velocity dispersion and the luminosity of the galaxy bulge. These tight relations point to the joint evolution of galaxies and SMBH (e.g. Fer-

rarese & Ford 2005).

A small percentage of galaxies ($\sim 1\%$) called Active Galactic Nuclei (AGNs) shows a SMBH active in their centers because of the release of gravitational energy of the gas surrounding the SMBH due to accretion, as radiation from IR to X-ray band. Since the gas temperature reaches $\sim 10^5$ K the energy is emitted as UV-X ray radiation. Likely a fraction of this energy is re-emitted as IR radiation by dust around the SMBH.

Only a small fraction of all AGNs ($\sim 10\%$) shows significative emission in radio band. This subclass of AGNs, called radio-loud AGNs, show the presence of a jet of matter propagating out to kpc or Mpc from the center. Although it is not fully explained, the radio-laud/radio-quite division seems to be linked with the spin of the SMBH (Rees 1984).

Radio-loud AGNs can be divided in extended radio sources (those shown a resolved structure when observed with a single radio telescope) and compact sources.

Historically, extended radio sources have been classified in two classes by Fanaroff and Riley (1974) in terms of the separation between the brightest parts of their radio lobes: Fanaroff-Riley type I (FRI) and Fanaroff-Riley type II (FRII) sources.

FRI radio galaxies show symmetric radio jets with high brightness near the galaxy core, decreasing in outer regions. On the contrary, FRII sources display two well distinct bright lobes at distances of the order of even Mpc far from the core, the so-called hot spots. The jets connecting the lobes are often too faint to be detected.

Furthermore FRI sources lack strong emission lines that instead are observable in FRII sources.

The physics underlying the FRI/FRII distinctions is based on the speed and propagation of the jet that is likely linked to different regimes (radiatively efficient/inefficient) of the accretion flow on the SMBH (Ghisellini & Celotti 2001). In FRI sources jets become quickly transrelativistic instead in FRII

radio galaxies are highly relativistic.
If the jet of the radio-galaxy point to the observer, the observer sees a compact source, with high variability and polarization in radio band, with a unresolved core. This kind of radio sources are called blazars.
Blazars are radio-loud AGNs with:

- high variability at all frequencies;
- high optical and radio polarization (up to 20%);
- presence of a compact radio core.

Based on their optical spectra, blazars are divided in two classes: Flat Spectrum Radio Quasars (FSRQs) and BL-Lacertae objects (BL-Lacs). In contrast with FSRQs, BL-Lacs show absence(Equivalent Width < 5 Å) of emission lines in their optical spectra.
In the current unification paradigm for AGNs, where the different classification of AGNs is based on different viewing angle of the accreting SMBH, radio galaxies are the parent populations of blazars (Urry & Padovani 1995). In this scheme relativistic effects amplify the non-thermal beamed emission jet, pointing to the observer, producing the peculiar features of blazar spectra. According to Urry & Padovani (1995) FRI radio galaxies should be the parent population of BL-Lacs while FRII sources of FSRQs. Although the observational evidences of these predictions are not simple, morphological and environmental studies of radio AGNs (e.g. McLure et al. 1999) and the recent detection of γ-rays emission from radio galaxies (Abdo et al. 2010d) seem to validate the relation between blazars and radio galaxies.

2.2.2 The Blazar SED

Thanks to *EGRET*, it has been possible to describe the whole Spectral Energy Distribution (SED) up to GeV band. Two are the main features:

- the double humped shape of the SED characterized by the first peak due to the synchrotron emission of electrons in the jet and the second peak made by IC scattering of jet electrons on a low energy photon field whose nature will be explained later;

- the total energetic output largely dominated by the high energy component

Fossati et al. (1998) constructed average SEDs binning the objects according to their radio luminosity (at 5 GHz) irrespective of their optical classifications and fitting the SEDs with an analytic parametrization. It turns out that for each bolometric luminosity the SED shows two distinct bumps, the first peaking between $10^{13} - 10^{17}$Hz, while the second between $10^{21} - 10^{24}$Hz. Increasing the bolometric luminosity the two peaks shift to lower energy following the so called "blazar sequence" (Fig. 2.1). The theoretical explanation of the phenomenological "blazar sequence" has been given by Ghisellini et al. (1998) in terms of different radiative cooling suffered by the emitting electrons in the jet with different power.

2.2.3 Emission mechanisms

As pointed out before, blazars are identified as radio-loud AGNs with a relativistic jet pointing along the observer's line of sight. The population of relativistic electrons in the jet is responsible of the peculiar blazar shape. As demonstrated by the high degree of polarization, the first peak is due to synchrotron emission coming from relativistic electrons and magnetic field in the jet. More complicated is the explanation of the second bump at higher energy. The most common theoretical models are hadronic and leptonic models.

In the leptonic models the same electrons responsible for synchrotron emission up-scatter via Inverse Compton (IC) a lower energy photon field. Different sources of soft photons can be taken into account. In the Synchrotron-Self

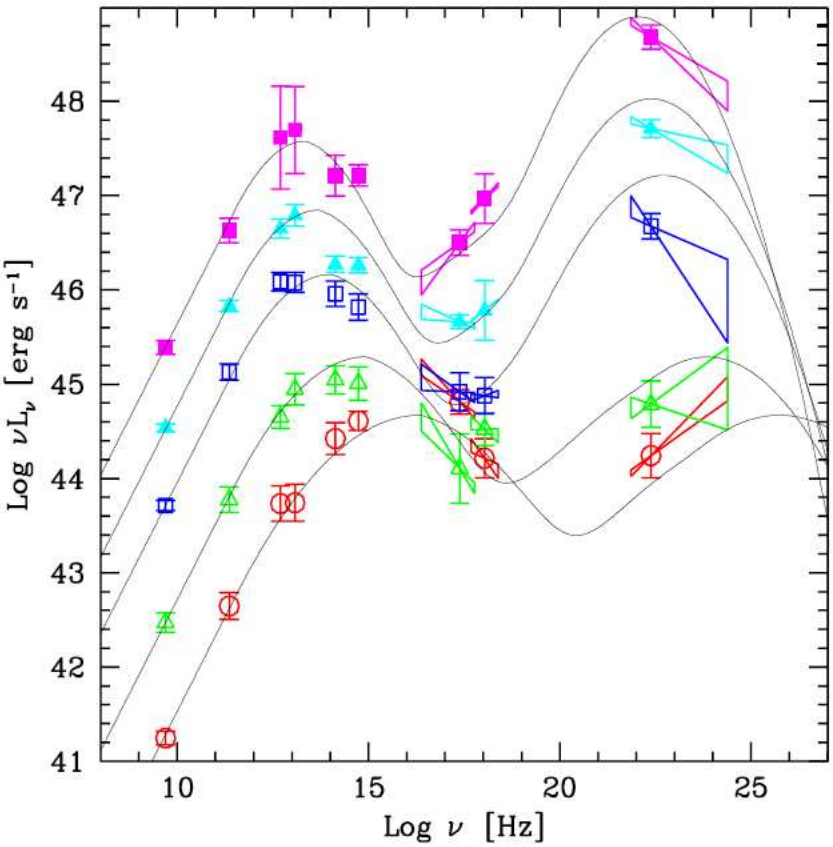

Figure 2.1: The average SEDs computed by Fossati et al. (1998) as displayed in Donato et al. (2001)

Compton model (SSC) (e.g. Maraschi Ghisellini & Celotti 1992) relativistic electrons interact via IC scattering the same photons created by synchrotron emission. In this framework Synchrotron and IC emission are then closely linked.

Differently in the External Compton model (EC) the target photon field assumed to dominate over the synchrotron photons, is due to soft photons coming from the central region of the AGN (Dermer & Schlickeiser 1993; Blazejowski et al. 2000).

Are totally different the Hadronic models. Their basic feature is the presence of a populations of high energy (in the TeV band) protons accelerated in the jet that interact with soft photons via pair production (e.g. Mannheim 1993) initiating a pair cascade. Successive populations of pairs of lower energies (down to MeV) will produce the observed γ-ray emission. Such models have been used to explain the behavour of BL-Lacs.

2.2.4 Blazars in γ-ray band

In this section we review observed properties of blazars in the γ-ray band. Blazars are the most common objects in the γ-ray sky. This was the main result of nine years of observations by *EGRET* (Hartman et al. 1999). The telescope measured 66 high confidence blazars 77% identified as FSRQs and 23% as BL-Lacs.

There are three the catalogs that collect *Fermi*-LAT observations of extragalactic sources:

- LBAS (LAT Bright AGN Sample) collects the brighter sources detected during the first three months of activity (2008 August 4 -October 30). It consists of 104 blazars detected within 10 σ, with 58 FSRQs, 42 BL-Lacs, 4 blazars with unknown classification and 2 radio galaxies. With this sample, a blazar γ-ray luminosity function has been extracted (Abdo et al. 2009);

- 1LAC (First LAT AGN Catalog) includes 671 γ-ray sources located at high Galactic latitudes (b $> 10^o$) detected at 5 σ. Some LAT sources are associated to multiple AGNs so the catalog includes 709 AGNs including 300 BL-Lacs, 296 FSRQs, 41 AGNs of other types and 72 AGNs of unknown type (Abdo et al. 2010e);

- 2LAC (Second LAT AGN Catalog) delivered in September 2011 it collect AGN observations over three years. The clean sample includes 395 BL-Lacs, 310 FSRQ and 156 unknown sources (The *Fermi* collaboration 2011).

Although many bright LAT blazars show breaks in their γ-ray band, the fit over the whole LAT band is useful to determine the photon spectral index Γ. At faint fluxes Fermi-LAT detects more easily hard spectrum sources rather then soft spectrum sources. To overtake this strong selection bias (Abdo et al. 2010e and The *Fermi* collaboration 2011) studied a sample of fluxes $F_{100} > 7 \times 10^{-8}$ph cm^{-2} s^{-1} where F_{100} is the flux over 100 MeV. Above this flux limit *Fermi*-LAT detects 135 sources with a photon index distribution compatible with a Gaussian with mean 2.40$\pm$0.02 and dispersion 0.24$\pm$0.02. From this sample FSRQs are more steeper than BL-Lacs with an average photon index of 2.42$\pm$ 0.17 compared to 2.0 $\pm$ 0.14 (see Fig. 2.2).
From the 2LAC Clean Sample, the *Fermi* collaboration provides the FSRQ and BL-Lac redshift distributions. FSRQs display a smooth redshift evolution with a peak at redshift $z \sim 1$ instead BL-Lacs show an abrupt decrease up to $z \sim 0.5$ (see Fig. 2.3).

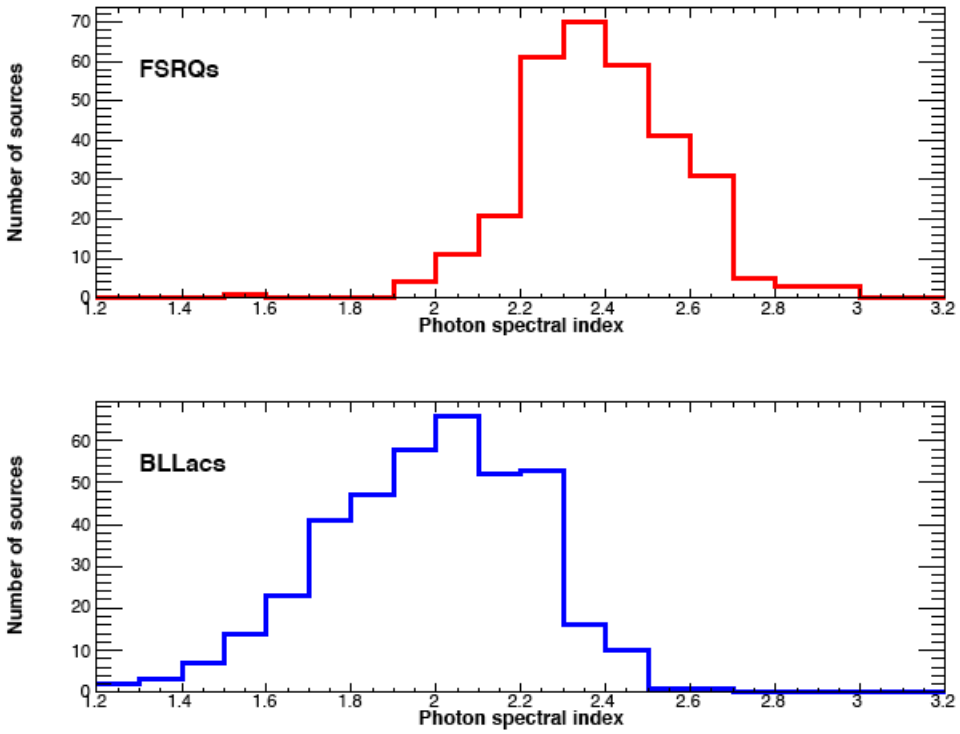

Figure 2.2: The photon index distribution for FSRQs (upper panel) and BL-Lacs (bottom panel) from the 2LAC (The *Fermi* collaboration 2011)

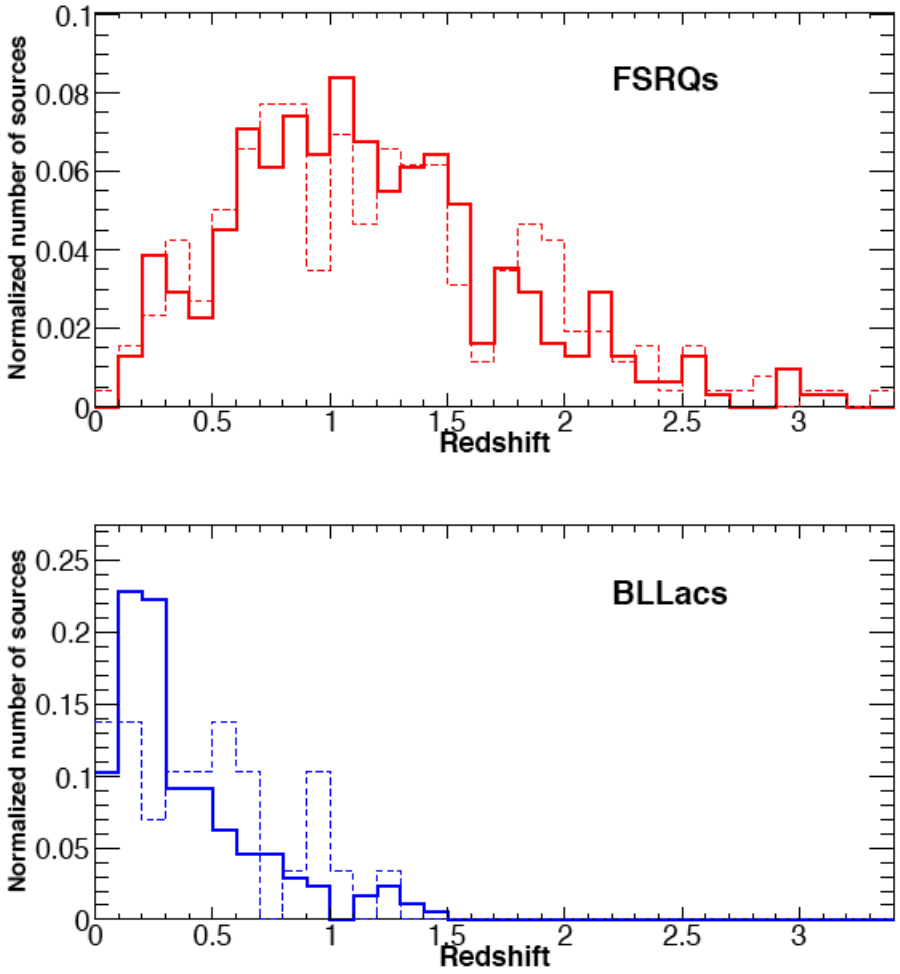

Figure 2.3: Comparison between redshift distributions for blazars in the 2LAC Clean Sample (solid) and the 5-Year WMAP complete sample (dashed). Top: FSRQs. Bottom: BL Lacs. (From the *Fermi* collaboration 2011)

2.3 The *Fermi*-LAT EGB

In this section we present the first measurement of EGB [1] derived in the energy band (200 MeV-100 GeV) from the *Fermi*-LAT data obtained after 10 months of observations (Abdo et al. 2010a).

The EGB value is strongly dependent on the model of the Diffuse Galactic Emission (DGE), the γ-ray emission from cosmic rays (CR) interacting with the Galactic interstellar gas and radiation fields. The DGE model depends on the propagation on CR inside the Milky Way, that is strictly parameter dependent. The solar emission and the CR background is subtracted to the total γ-rays photon detected by *Fermi*-LAT obtaining the total EGB containing the resolved source component and unresolved or genuinely diffuse component.

The EGB intensity extrapolated to 100 MeV based on the power law fit is I(>100 MeV)=1.42 $\times 10^{-5}$cm^{-2}s^{-1}sr^{-1} where resolved sources accounts for $\simeq$ 27% of the emission, the rest being ascribed to the diffuse component (see Fig. (2.4)). Furthermore it is worth noting that the diffuse component spectrum is compatible with a featureless power law with photon index $\Gamma = 2.41 \pm 0.05$.

2.4 The Blazar contribution to EGB

The blazar contribution (in photons s^{-1} cm^{-2} sr^{-1} MeV^{-1}) to the EGB at the observed energy E_0 is

$$I_{\rm blaz}(E_0) = \frac{1}{4\pi}\int_0^\infty dz \frac{dV}{dz}\int_{\log L_\gamma^{\rm min}}^{\log L_\gamma^{\rm max}} d\log L_\gamma \frac{d\Phi_\gamma(L_\gamma,z)}{d\log L_\gamma} \times \frac{dn(L_\gamma,z)}{dE} e^{-\tau_{\gamma\gamma}(E_0,z)}, \quad (2.4.1)$$

where $d\Phi_\gamma(L_\gamma,z)/d\log L_\gamma$ is the γ-ray Luminosity Function (LF) and L_γ is νL_ν (in erg/s) at 100 MeV, $dn(L_\gamma,z)/dE$ is the unabsorbed photon flux per

[1] We refer here to EGB as the superposition of contribution coming from resolved extragalactic sources and a truly diffuse component.

unit energy $E = E_0(1+z)$ measured on Earth of a blazar with luminosity L_γ at redshift z, and $\tau_{\gamma\gamma}(E_0, z)$ is the optical depth for $\gamma - \gamma$ absorption. We adopt the EBL model by Finke, Razzaque, & Dermer (2010) (see chapter 4). In the above equation dV/dz is the comoving cosmological volume [2]. We set $\log L_\gamma^{\rm min} = 43.5$ and $\log L_\gamma^{\rm max} = 50$.

The number of sources $N(> F_{\rm ph})$ per steradian with photon flux greater than $F_{\rm ph}$ is

$$N(> F_{\rm ph}) = \frac{1}{4\pi} \int_0^\infty dz \, \frac{dV}{dz} \int_{\log L_\gamma^{\rm min}}^{\log L_\gamma^{\rm max}} d\log L_\gamma \, \frac{d\Phi_\gamma(L_\gamma, z)}{d\log L_\gamma}. \tag{2.4.2}$$

The γ-ray LF of blazars is presently uncertain (for an estimate see, e.g., Abdo et al. 2009), so that one has to rely on the LFs computed in other bands, e.g., X-rays (Narumoto & Totani 2006; Inoue & Totani 2009; Abazajian, Blanchet, & Harding 2010a), or radio (Draper & Ballantyne 2009; Stecker & Venters 2010). We adopt here the radio LF at 151 MHz of FRI and FRII (Willott et al. 2001, see Fig. 2.6), assumed to be the parent populations of blazars:

$$\frac{\Phi_\gamma(L_\gamma, z)}{d\log L_\gamma} = \kappa \, \frac{\Phi_R(L_R, z)}{d\log L_R}, \tag{2.4.3}$$

where $L_{\rm R}$ is νL_ν at 151 MHz, and the constant κ is the fraction of blazars over all radio galaxies, and it is our fit parameter. In order to convert radio into γ-ray luminosity, we must rely on the blazar spectral energy distribution (SED). We use the SEDs computed by Inoue & Totani (2009) based on the empirical determinations of Donato et al. (2001). The relation between radio luminosity (151 MHz) and γ-ray luminosity (100 MeV) is shown in Fig. 2.5.

[2] We adopt here and in the next chapters the following cosmological parameters: $H_0 = 70$km/s/Mpc Ω_m=0.3 and Ω_Λ=0.7

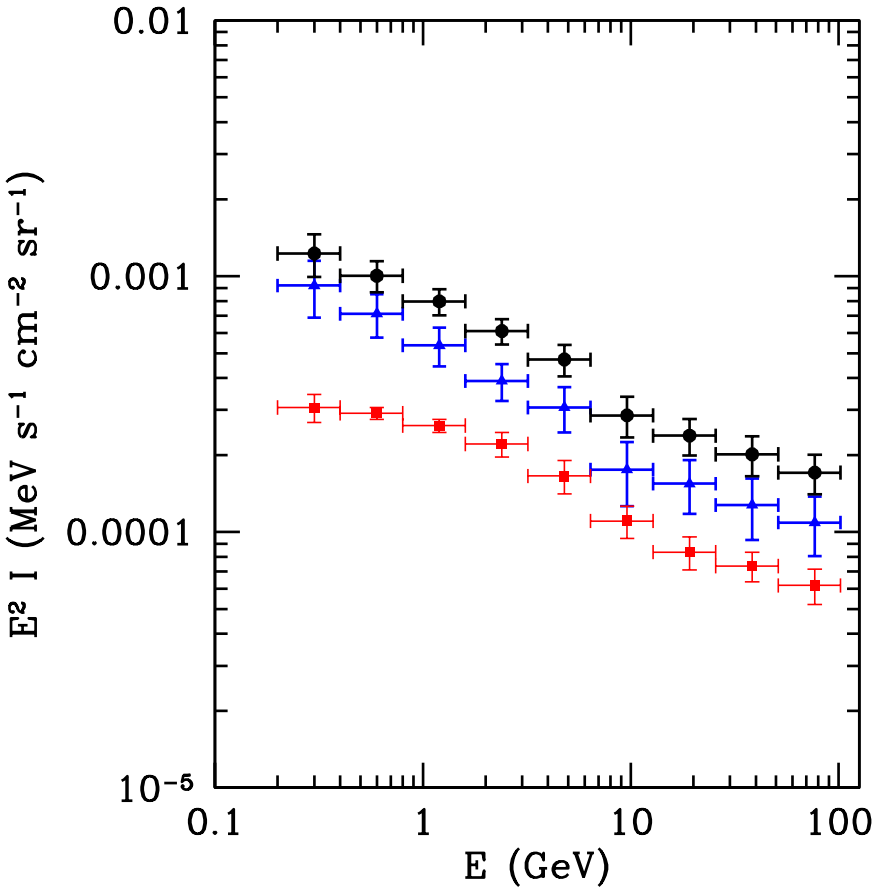

Figure 2.4: The EGB measured by *Fermi*-LAT. Red points are the resolved source component, blue point the diffuse component and black points are the total EGB.

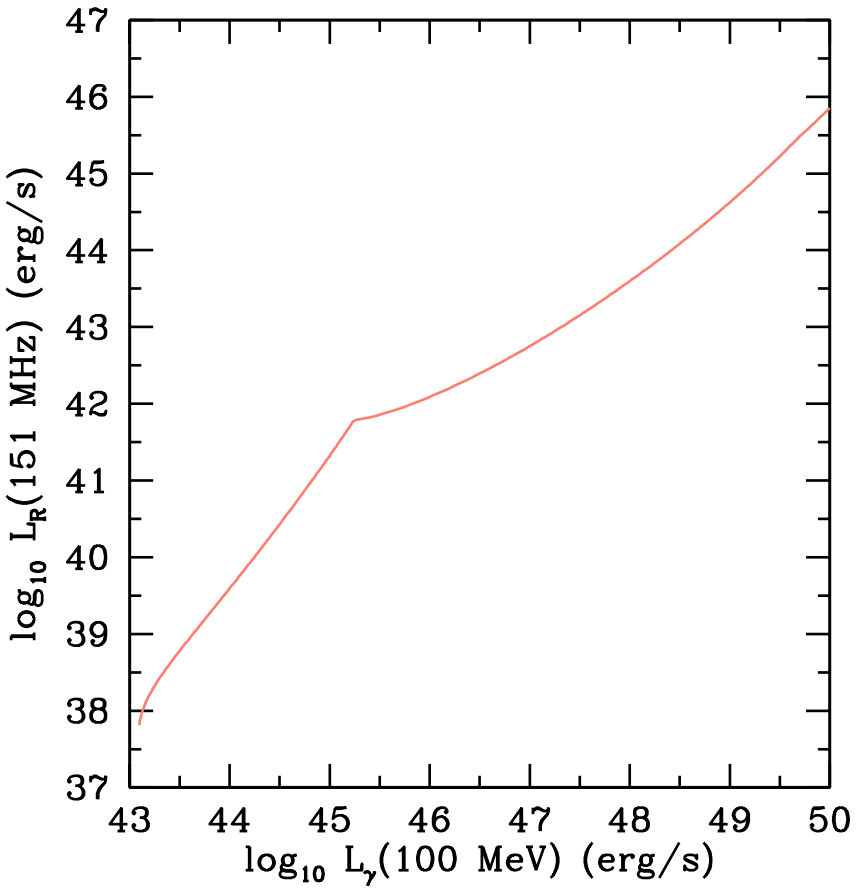

Figure 2.5: The relation between L_γ at 100 MeV and L_R at 151 MHz obtained by the SED (Fossati et al. 1998)

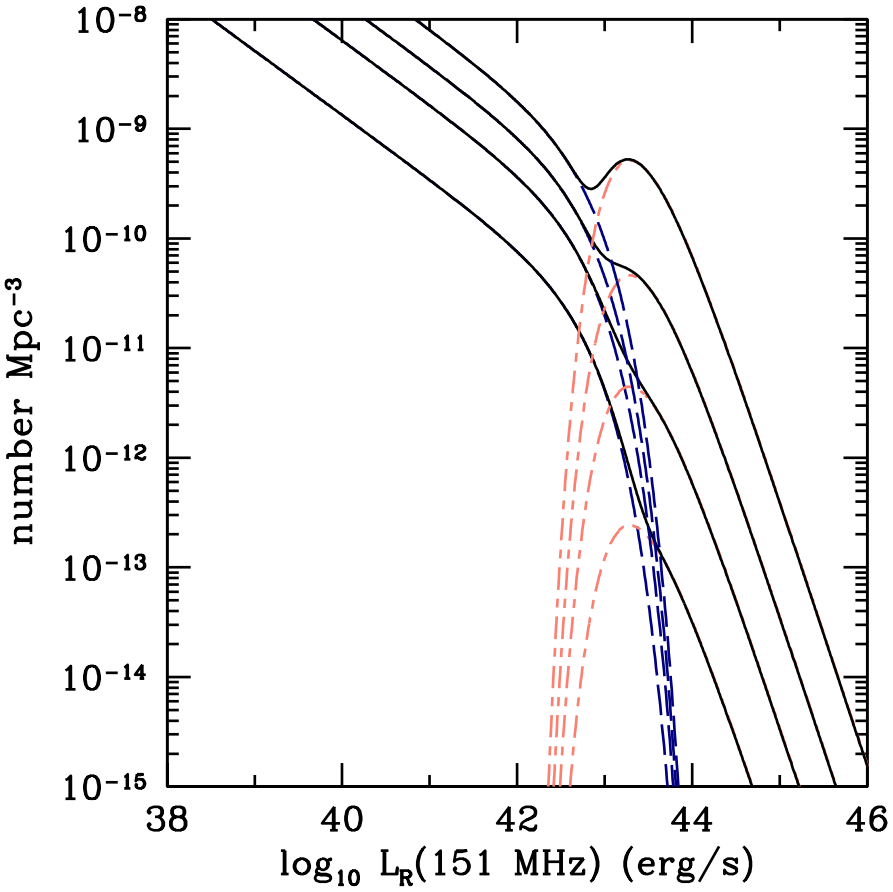

Figure 2.6: The Radio LF at 151 MHz derived by Willott et al. 2001 at different redshifts (z=0, 0.5, 1, 2, from the bottom) for FRI sources (dashed blue line) and FRII source (dotted-dashed red line) and the sum (black).

2.5 Results

We use the model discussed in the previous section to compute the total contribution of blazars (FSRQs and BL-Lacs) to the *Fermi*-LAT EGB. The best fit parameter value we obtain is $\kappa = (3.93 \pm 0.01) \times 10^{-4}$. The number ratio of blazars to radio galaxies κ can be thought as a measure of the beaming factor of the relativistic jet, which in turn is related to the bulk Lorentz factor Γ. From $\kappa \sim 1/2\Gamma^2$ we derive $\Gamma \sim 35$.

Fig. 2.8 shows the corresponding contribution of FSRQs and BL-Lac to the total *Fermi*-LAT EGB. The background intensity is found to be $I_{\rm FSRQ} = 4.22 \times 10^{-6}$ph s^{-1}cm^{-2}sr^{-1} and $I_{\rm BL-Lac} = 2.43 \times 10^{-6}$ph s^{-1}cm^{-2}sr^{-1} for FSRQs and BL-Lacs respectively. The total EGB intensity is therefore $I = 6.65 \times 10^{-6}$ph s^{-1}cm^{-2}sr^{-1}, corresponding to 45% of the one measured by *Fermi*-LAT.

From the slope of the FSRQ and BL-Lac component in Fig. 2.8 we can see that the main photon index of FSRQs and BL-Lacs resulting from our model are in agreement with the 2LAC (The Fermi collaboration, 2011).

We note that blazars fall short to explain the measured EGB at E<10 GeV and at E>50 GeV. At low energies, the discrepancy can be fully accounted by star-forming galaxies modeled following the recipes by Stecker & Venters (2010), so that only the last point of the *Fermi*-LAT EGB measurement is not reproduced by our blazar model.

We assess that a galactic DM component could in principle account for the 70-100 GeV point. The two following sections show the star-forming model and the DM model we adopt.

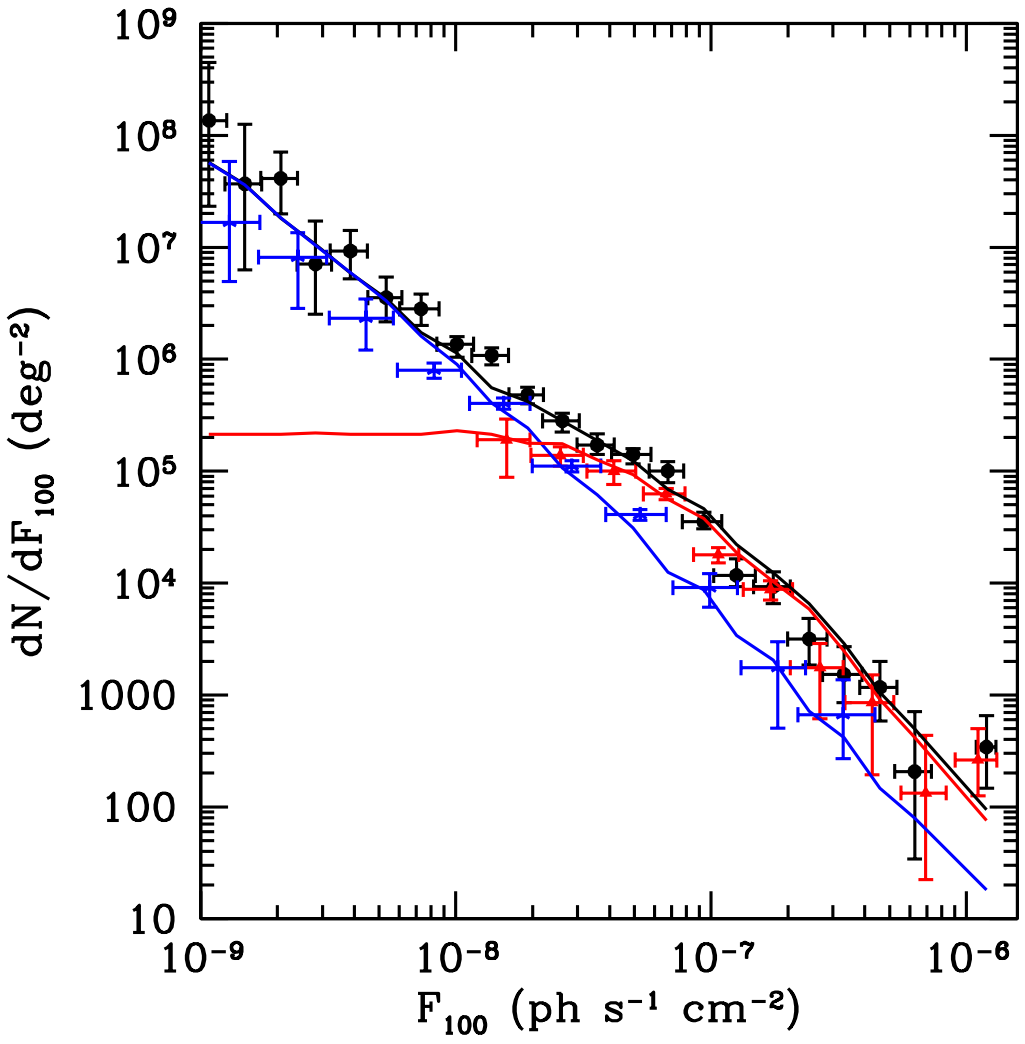

Figure 2.7: The black line represents the fit to blazar logN- logS measured by Fermi (Abdo et al. 2010) as a sum of BL-Lac component (blue line) and FSRQ component (red line). Black points are the number counts of all the blazars, red points FSRQs and blue points BL-Lacs.

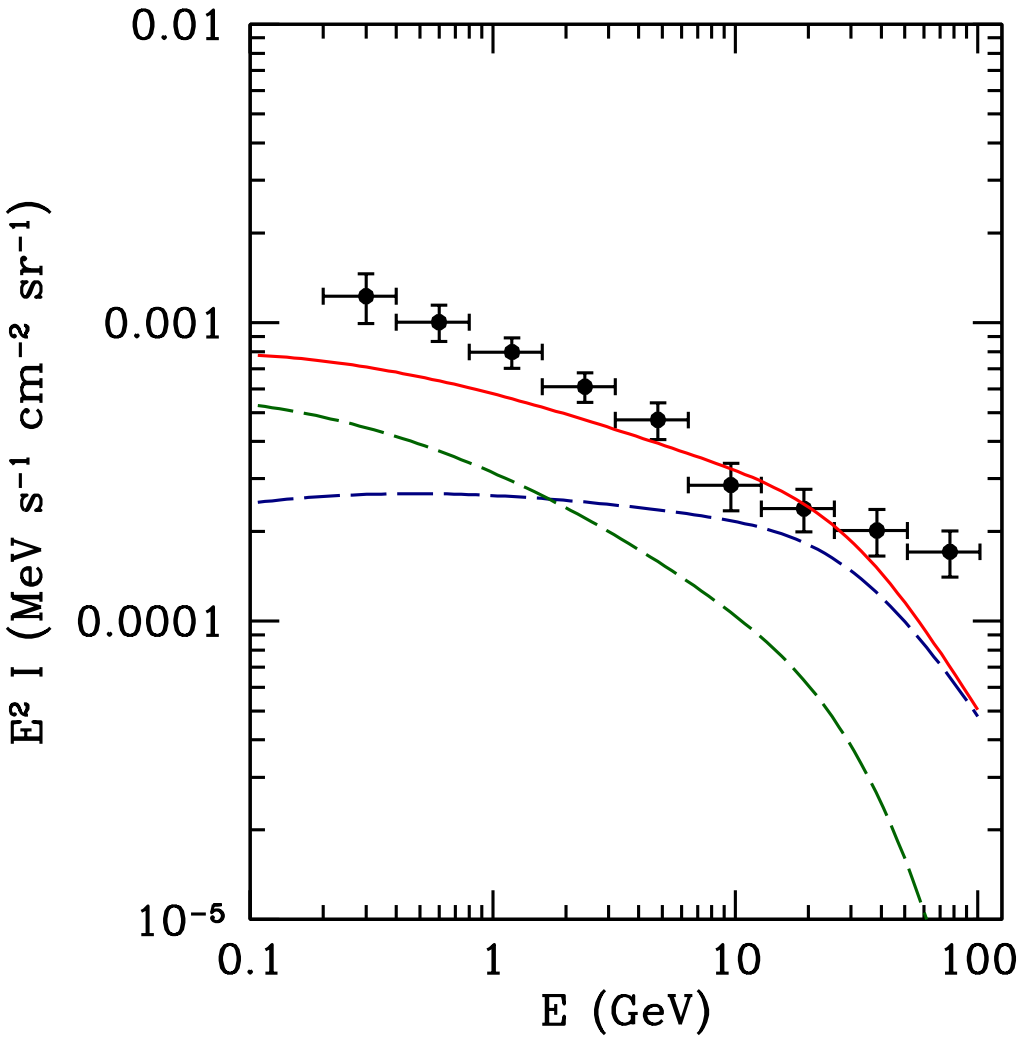

Figure 2.8: The black points represent the total EGB (resolved and unresolved sources and all the rest), blue line is the FSRQ component, the green line is the BL-Lac component. The red line is the sum of the two components.

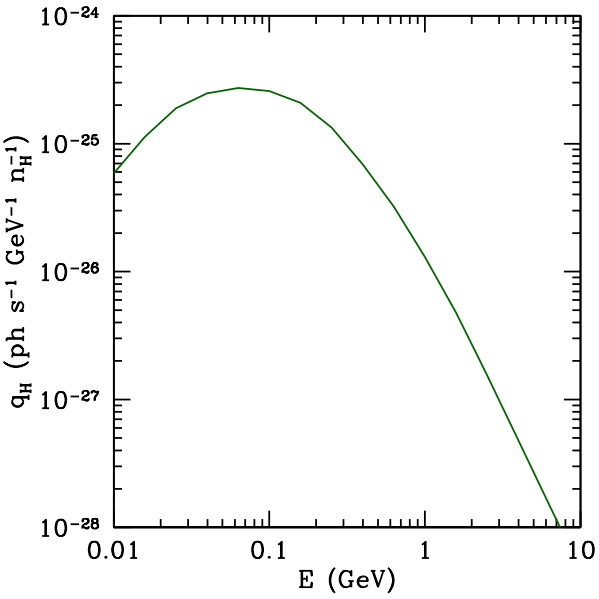

Figure 2.9: The pionic γ-ray production spectrum per hydrogen atom as a function of energy (Mori 1997).

2.6 Star-forming galaxy component

The γ-ray spectrum of a star-forming galaxy is based on the assumption that γ-ray emission is due to the decay of π^0 mesons. The π^0 mesons form in the inelastic collision between cosmic rays and the ISM. According to Stecker & Venters (2010), the specific γ-ray photon spectrum $L_{\rm ph}$ (photons s^{-1} MeV^{-1}) of a star-forming galaxy is related to the average pionic γ-ray production spectrum per hydrogen atom $\langle q_{\rm H}(E_0)\rangle$ (Dermer 1986; Mori 1997) (see Fig2.9) as,

$$L_{\rm ph}(E_0) = \langle q_{\rm H}(E_0)\rangle N_{\rm H}, \tag{2.6.1}$$

where $N_{\rm H}$ is the total number of hydrogen atoms in the galaxy, both in atomic and molecular form.

We adopt the *Strong Coupling γ-ray - Star Formation Rate Model* of Stecker & Venters (2011), where $N_{\rm H}$ is related to the star formation rate. According to the model, the star-forming galaxy contribution to the γ-ray

background is

$$I_{\rm gal}(E_0) = \frac{1}{4\pi}\int_0^\infty dz \frac{dl}{dz}\frac{(1+\mathcal{R})}{m_{\rm H}\xi(H_2)}\langle q_{\rm H}(E)\rangle\,\dot{\rho}_{\rm SFR}(z)e^{-\tau_{\gamma\gamma}(E_0,z)}, \qquad (2.6.2)$$

where $dl/dz = cH^{-1}(1+z)^{-1}$ with $H(z)$ the Hubble parameter, $\mathcal{R} \sim 0.9$ is the ratio of atomic-to-molecular hydrogen density in star-forming galaxies (see Leroy et al. 2008), and $\dot{\rho}_{\rm SFR}$ is the cosmic star formation rate (we use the fit proposed by Li 2008). The parameter $\xi(H_2)$ (the star formation efficiency of molecular hydrogen, see Bigiel et al. 2008, Gnedin et al. 2009) is the ratio between $\dot{\rho}_{\rm SFR}$ and the cosmic density of molecular hydrogen.

2.7 Dark Matter component

The existence of DM is well supported by its gravitational effect on the galaxy rotation curves and the dynamics of cluster of galaxies. It turns out also necessary in explaining the cosmological structure formation (see e.g. Peacock 1999). The most suitable DM candidates are non baryonic, i.d. beyond the particle Standard Model, and weakly interacting massive particles (WIMPs). Indirect DM searches focused on WIMPs annihilations in γ-ray band and EGB could in principle contain DM contribution, both galactic and extragalactic.

If DM consists of particles with mass $\rm m_{DM}$ and velocity-averaged cross section for annihilation $\langle\sigma v\rangle$, the number flux is (Ando 2005):

$$I_{\rm DM}^{\rm GC} = \frac{\langle\sigma v\rangle}{2}\frac{J}{J_0}\frac{1}{4\pi m_{\rm DM}^2}\frac{dn_\gamma}{dE} \qquad (2.7.1)$$

where

$$J = \frac{1}{8.5{\rm kpc}}\int dl \left(\frac{\rho(r(\psi,l)}{0.3{\rm GeV/cm^3}}\right)^2 \qquad (2.7.2)$$

where the integration in extended over the line of sight and the spectrum is computed following Ando (2005):

$$\frac{dn_\gamma}{dE} \simeq \frac{0.73}{m_{\rm DM}}\frac{e^{-7.76(E/m_{\rm DM})}}{[(E/m_{\rm DM})^{1.5}+0.00014]} \qquad (2.7.3)$$

The extragalactic DM contribution is given by:

$$I_{\rm EGB} = \frac{c}{4\pi H_0}\frac{\langle\sigma v\rangle}{2}\frac{\Omega_{\rm DM}^2\rho_{\rm crit}^2}{m_{\rm DM}}\int dz \frac{(1+z)^3}{H(z)}\frac{dN_\gamma}{dE}f(z)e^{-\tau_{\gamma\gamma}(E_0,z)} \qquad (2.7.4)$$

where $H(z)$ is the cosmological term while the term $f(z)$ accounts for the increase in density squared during halo growth and the redshift evolution of the halo mass function (see Abazajian, Blanchet, & Harding 2010b):

$$f(z) = f_0 10^{0.9[\exp(-0.9z)-1]-0.16z} \qquad (2.7.5)$$

with $f_0 \simeq 3\times10^4$ fixed by Einasto profile. Our total DM contribution (galactic plus extragalactic) is boosted by a factor of 6.6.
Fig. 2.10 shows the contribution to EGB of different annihilating DM particles.

2.8 Discussion and Conclusions

We have computed the overall contribution of blazars to the *Fermi*-LAT EGB.
Our model relies on two assumptions: the radio LF and the blazar SED. In the following we show the difference with the most reliable works on the contribution of blazars to the *Fermi*-LAT EGB.

- We use the radio LF of Willott (2001). Fitting the differential logN-logS we obtain just the overall normalization k, without any change on the bright and faint end of LF.
  In previous works (Narumoto & Totani 2006; Inoue & Totani 2009) it is assumed a LF in X band with three free parameters: the total normalization, the amount of bolometric radiation emitted in X-ray and the faint end of the X-ray LF. Differently in Stecker & Venters (2010) the radio LF computed by Dunlop & Peacock (1990) is used, changing the faint end to obtain the contribution of FSRQs.

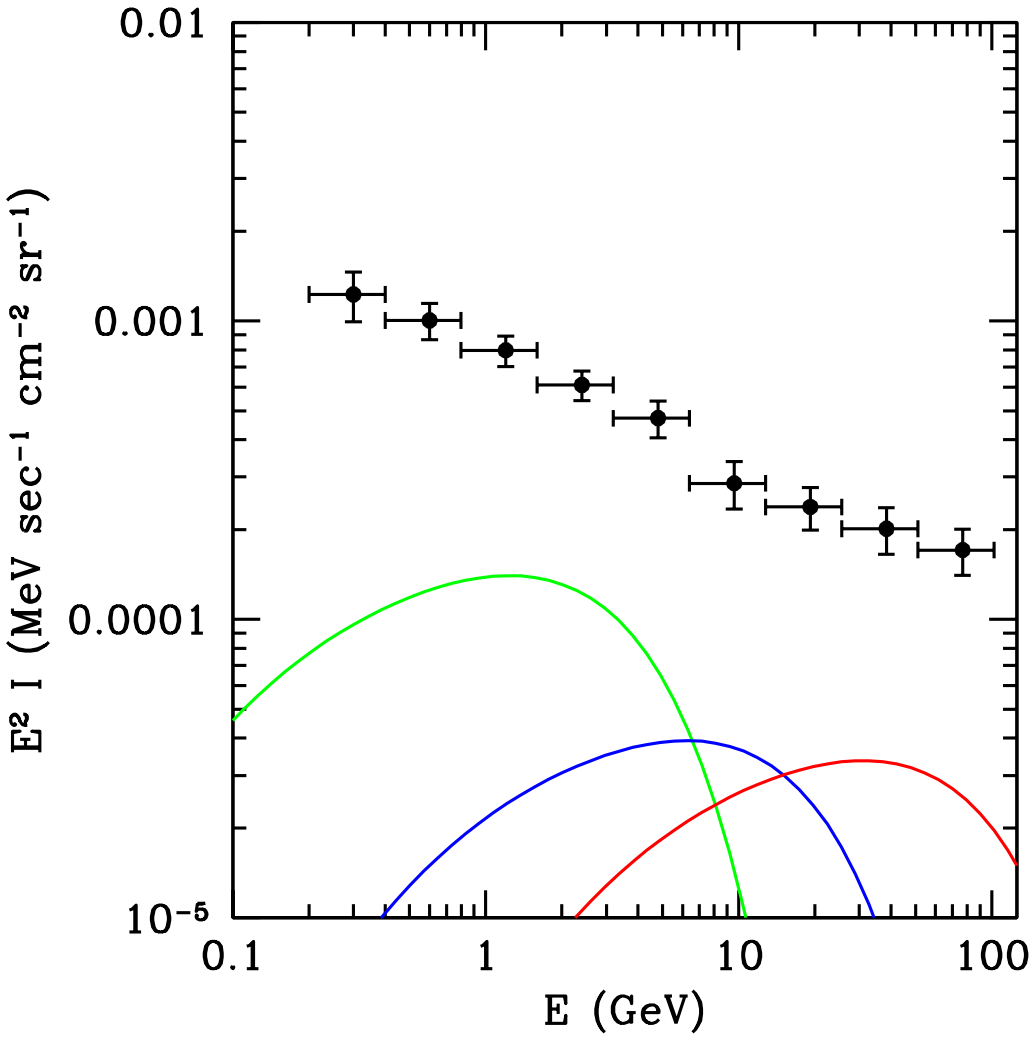

Figure 2.10: Annihilating DM component with different masses and cross sections: m_{DM}=20 GeV and $\langle\sigma v\rangle = 5\times10^{-26}$ cm^3 s^{-1} (green line), m_{DM}=100 GeV and $\langle\sigma v\rangle = 7\times10^{-26}$ cm^3 s^{-1} (blue line), and m_{DM}=500 GeV and $\langle\sigma v\rangle = 30\times10^{-26}$ cm^3 s^{-1} (red line).

- The second main point of our model is represented by the blazar SED. We assume that the spectra of blazar is fully taken into account by the *blazar sequence* (Fossati et al. 1998). On the contrary in Stecker & Venters (2010) it is assumed the blazar spectra as a simple and broken power law, respectively. In these works they assume a spectral index distribution peaked on the mean spectral index resulting from observations. The underlying assumption is that the unresolved blazar component has the same index distribution of the resolved component. Using the blazar sequence such assumption is not necessary because the blazar SEDs are fully determined.

The best fit value of the relative number of blazars with respect to radio galaxies can be translated into a bulk Lorentz factor of the relativistic jet $\Gamma \sim 35$, larger than the average value $\Gamma \sim 15$ estimated by Ghisellini et al. (2010). The two values could be reconciled if blazars commonly show secular γ-ray large variability which modulates the 1-year average flux, as recently proposed by Ghirlanda et al. (2011).
To be consistent with the *Fermi*-LAT points at lower energy, we add the star-forming component to our blazar model. Fitting the *Fermi*-LAT EBG with this two component model, we constrains the so-called " star formation efficiency of molecular hydrogen" $\xi = 7.0 \times 10^{-10}\mathrm{yr}^{-1}$, which we found well within existing, much looser observational constraints (Leroy et al. 2008). Fig 2.11 shows our best fit with the two component model.

Clearly, the specific best fit values obtained depend upon the details of our model, in terms of star formation rate adopted, models for the γ-ray emission of star-forming galaxies, blazar LF and SED. Nevertheless the overall picture appears quite robust, with non vanishing role played by star-forming galaxies, with blazars dominating mostly at the higher energies probed by *Fermi*-LAT. Though our model is statistically fully acceptable, it is interesting to note that the highest data point of the EGB (see Fig. 2.11) lies above our best fit model. In the energy band 50-100 GeV absorption of γ-rays

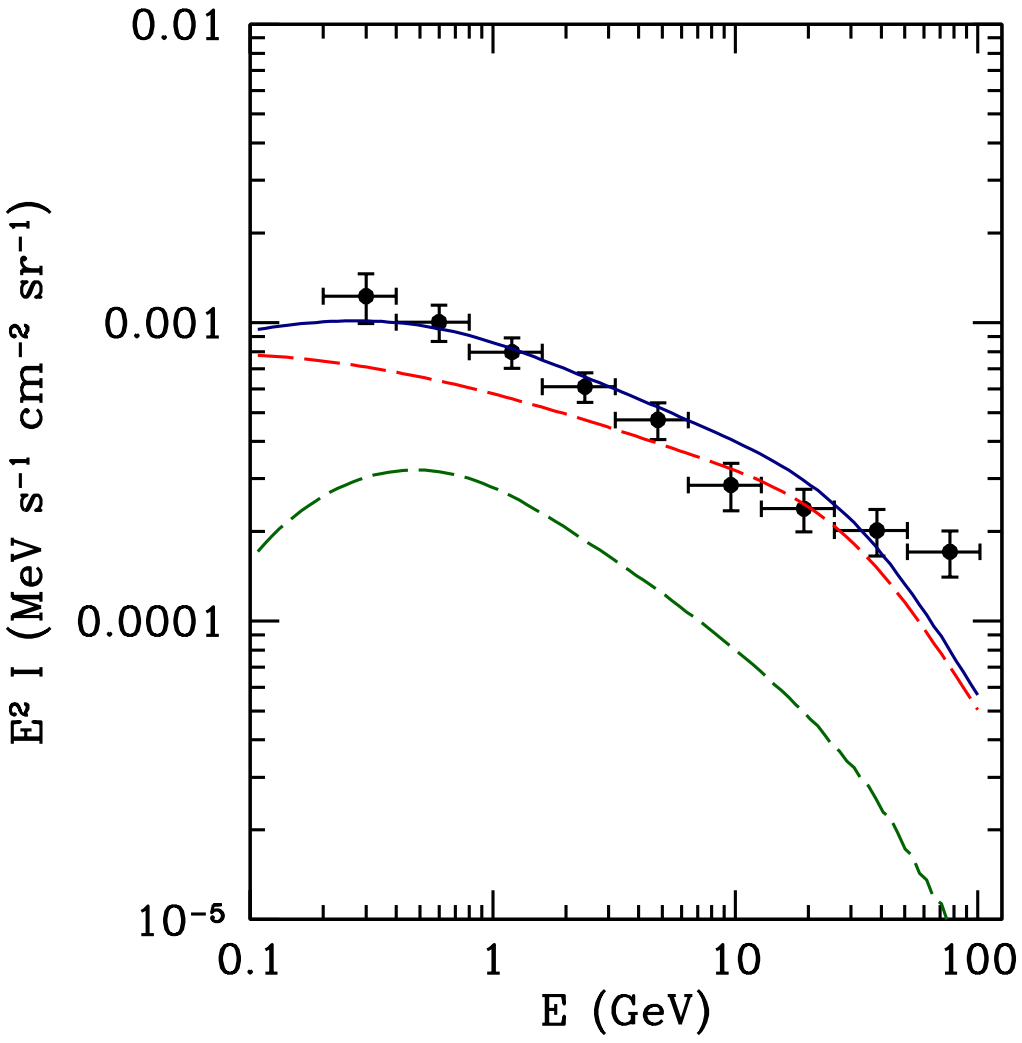

Figure 2.11: The star-forming galaxy component (green line), the total blazar component (red line) and the sum (blue line). In black are the *Fermi* EGB points.

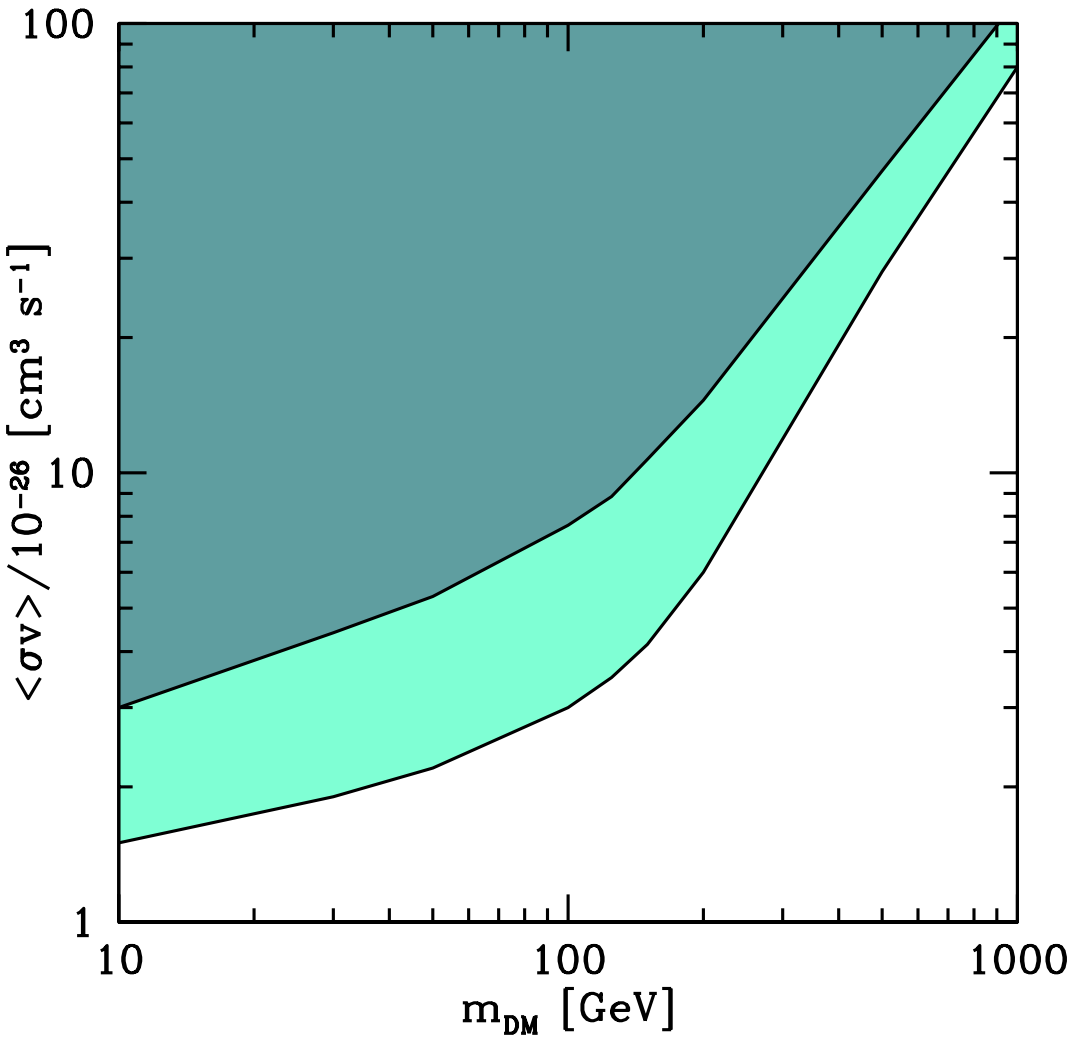

Figure 2.12: Upper limits of the cross section $\langle\sigma v\rangle$ as a function of particle mass m_{DM} for annihilating DM. The lower (upper) curve represents the 1(2)-σ limit. See text for details.

due to the interaction with the EBL is significant. Different theoretical EBL models have been proposed in the last few years (see chapter 4) resulting in somewhat different optical depth for photon-photon interaction. As already discussed, we follow Finke, Razzaque & Dermer (2010), and we checked that even adopting the model of Kneiske & Dole (2010), which gives the lowest γ-ray absorption, our EGB model still falls short in the 70-100 GeV range. A possible, intriguing explanation is the presence of an extra emission from annihilating DM particles (see, e.g., Ullio et al. 2002). Recently, Abazajian, Blanchet, & Harding (2010b) performed a detailed analysis of possible DM candidates in the context of *Fermi*-LAT EGB. For illustrative discussion, here we adopt the specific annihilating DM model shown in section 2.7, and compute its contribution to the EGB. We found, as an example, that a particle of mass $\simeq 0.5$ TeV and cross section $\langle \sigma v \rangle \simeq 5 \times 10^{-26}$ cm^3 s^{-1} can easily accomodate the last data point. However its presence is not statistically required by the fit, so it is fair to consider only upper limits to the DM component. Fig. 2.12 shows our results in terms of cross section $\langle \sigma v \rangle$ and particle mass $m_{\rm DM}$. The lower (upper) curve is computed by adding the DM background to our EGB model, allowing a χ^2 increase of 1 (4) with respect to the best fit, hence representing the 1(2)-σ upper limits of $\langle \sigma v \rangle$ for a given $m_{\rm DM}$. As an example, assuming $\langle \sigma v \rangle = 3 \times 10^{-26}$ as required for leaving the observed relic density of DM (Jungman, Kamionkowski, & Griest 1996), we can exclude at 1(2)-σ level DM particles with $m_{\rm DM} \sim 100(10)$ GeV. More massive particles can have a larger cross section, and still be compatible with EGB data. Our limits are consistent with other, more refined, determinations (e.g. Abazajian, Blanchet, & Harding 2010b)

Chapter 3

The intergalactic magnetic field

3.1 Introduction

Magnetic fields pervade the Universe. They exist in stars, galaxies, cluster of galaxies and in the intergalactic medium.
Contrary to the electromagnetic radiation, magnetic fields need indirect measure methods to be detected and for this reason it is difficult to give a precise estimation of their value.
Even if the origin of these fields has not been fully understood, according to the most common hypothesis, the magnetic fields of galaxies and cluster of galaxies result from the amplification of a pre-existing seed via dynamo or battery effect during the cosmic history.
Two are the possible explanations of the seeds: astrophysical or cosmological. According to the astrophysical hypothesis the seeds have been produced in pro-galaxies by the Biermann battery mechanism (Biermann 1950) that works when a ionized gas is in centrifugal equilibrium with strong interaction between protons and electrons. Implementing this mechanism to galaxies at high redshift results in a seed magnetic field B$\sim 10^{-20}$G (Pudritz &Silk 1989; Kulsrud et al. 1997; Gnedin et al. 2000).
Differently magnetic field seed can be produced during inflation, during the neutrino-photon decoupling or during phase transitions in the Early Universe

(Grasso & Rubistein 2001; Widrow 2002).

The intergalactic magnetic field (IGMF), the magnetic field not associated with collapsing or bound systems, represents an important tool to discriminate between astrophysical and cosmological origin of the magnetic field. A detection of sufficient strong IGMF would provide support to the cosmological hypothesis while the detection of very tiny fields would support the dynamo paradigm.

Only upper limits on IGMF exist so far obtained using the Faraday rotation technique, from the CMB spectrum and from limits on the Big Bang Nucleosynthesis.

γ-ray astrophysics provide a new method to compute a lower limit on the strength of the IGMF using blazars as a probe.

The basic idea, already predicted by Plaga (1995), is simple. Let suppose to have a TeV source, namely a blazar. Interacting with EBL TeV photons produce electron-positron pairs. These pairs interact with the CMB photons by IC scattering. The resulting photons have GeV energy and can be again absorbed by EBL starting a cascade. In absence of magnetic field the pairs are created along the line of sight and therefore the telescope measure direct TeV photons and secondary GeV photons. It results that the detection/ non-detection of GeV photons from a TeV source provide a lower limit on the value of the IGMF along the line of sight. The most suitable blazars are those detected in TeV band and not detected in GeV band, at a sufficient cosmological distance with an hard spectrum, e.g. 1ES 0229+200 (z=0.14), 1ES 1101-232 (z = 0.186), 1ES 0347-121 (z = 0.185). In particular almost all study on this technique use the blazar 1ES 0229+200 (see section 3.5) (Neronov & Vovk 2010, Tavecchio et al. 2010; 2011) and the resulting lower limit is $B_{IGMF} > 10^{-15}$G.

Implicit in all these studies is that the TeV blazars used to infer the IGMF emit constant flux over a long period of time. Because blazars are highly variable, a more defensible limit is obtained by assuming that the TeV radiation

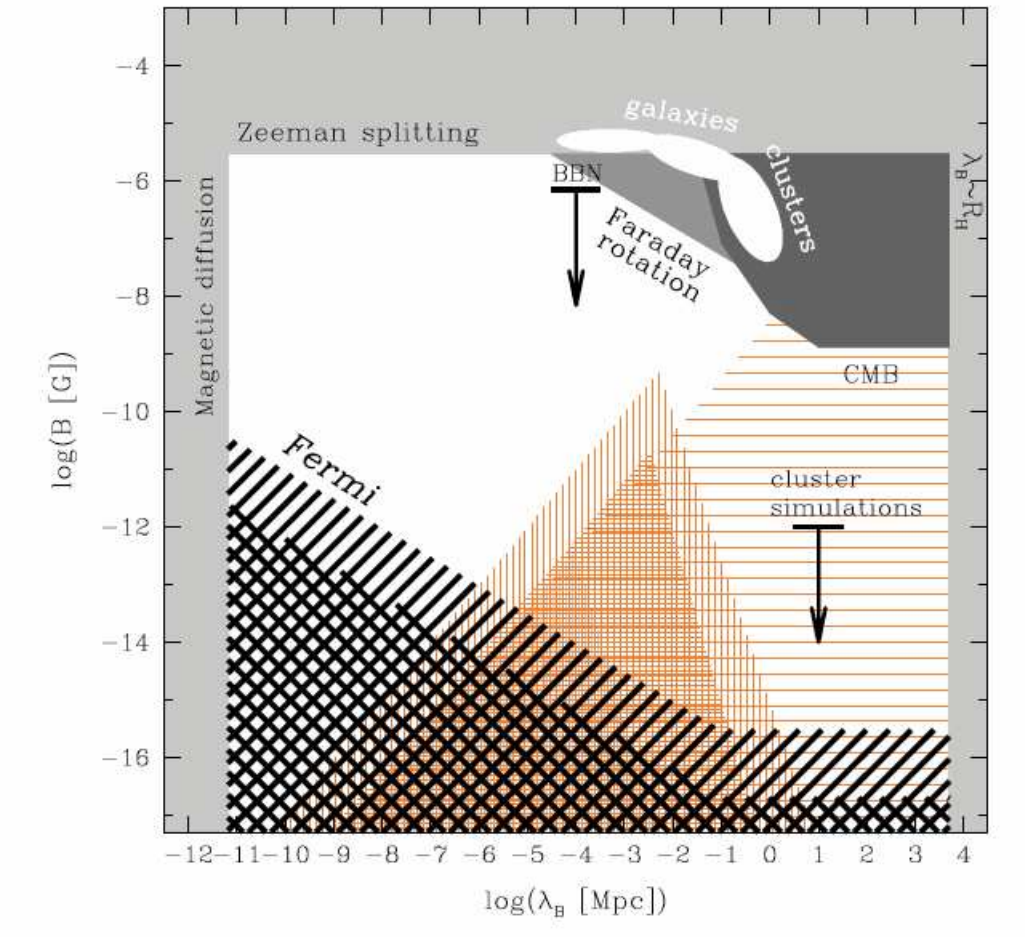

Figure 3.1: Figure shows the observational bounds of IGMF (see Neronov & Vovk 2010).

is emitted only over the past few years during which it has been monitored. A simple semi-analytical approach is used to derive a new minimum values for $B_{IGMF} > 10^{-19}$G.

In section 3.2 a brief review on the observational methods used to constrain the IGMF is provided (see 3.2). Section 3.5 shows the semi-analytical model used and section 3.6 shows the results. Conclusions are reported in section 3.7

3.2 Observations

Before entering into the details of the observations, it is worth noting that the value of the magnetic field is tightly linked with its coherence lengths λ_{ch}, defined as the lengths over which magnetic field direction changes of a $\pi/2$ factor. All inferred value of the magnetic field are fully dependent on the assumption of a precise value of λ_{ch}.
Following Widrow (2002), observations of galactic and extragalactic magnetic field can be summarized as follows:

- spiral galaxies show magnetic field with strength ~ 10 μG with a coherence length comparable to the radius of their disk;
- elliptical galaxies show random oriented magnetic fields with a coherence length smaller than the galactic scale;
- magnetic fields with strength of few microgauss have been detected in the intergalactic medium inside galaxy cluster with coherence length of the order of few kpc;
- as there is no direct detection of IGMF, constraints have been derived by considering its effect on big bang nucleosynthesis, the CMB and polarized radiation from extragalactic sources.

IGMF is measured in four ways: by Faraday rotation, by the study of the CMB anisotropies, by the effect on the Big Bang Nucleosynthesis and by the cascade emission from blazars. Note that in the following paragraphs we refer to IGMF as the cosmic magnetic field at redshift z=0.

3.2.1 Constraints from Faraday Rotation

Basically Faraday rotation occurs when polarized electromagnetic radiation travels through a magnetized medium.
In particular in the astrophysical environment radiogalaxies are used as

sources of polarized radiation. Along the path, if the intergalactic medium is magnetized the polarization vector rotate by an angle

$$\phi = \frac{e^3\lambda^2}{2\pi m_e^2 c^4}\int_0^{l_s} n_e(l)B_{\parallel}(l)dl + \phi_0 \tag{3.2.1}$$

where e, m_e are the electron charge and mass, respectively; λ is the wavelength of the radiation and ϕ_0 the initial phase. $B_{\parallel}$ and n_l are the magnetic field and the electron density along the line of sight, respectively.

In terms of rotation measure (RM) the equation reads:

$$\phi = (RM)\lambda^2 + \phi_0 \tag{3.2.2}$$

where:

$$\begin{aligned} RM &= \frac{e^3\lambda^2}{2\pi m_e^2 c^4}\int_0^{l_s} n_e(l)B_{\parallel}(l)dl \\ &\sim 810\int_0^{l_s}\left(\frac{n_e}{\mathrm{cm}^{-3}}\right)\left(\frac{B_{//}}{\mu\mathrm{G}}\right)\left(\frac{dl}{\mathrm{kpc}}\right)\left[\frac{rad}{m^2}\right] \end{aligned} \tag{3.2.3}$$

For a source at cosmological distance l_s, the RM is given by the generalization of eq. (3.2.3) including the expansion of the Universe:

$$RM \simeq 8.1\times 10^5\int_0^{l_s}\left(\frac{n_e}{\mathrm{cm}^{-3}}\right)\left(\frac{B_{\parallel}(l)}{\mu\mathrm{G}}\right)(1+z)^{-2}\frac{dl}{\mathrm{Mpc}} \tag{3.2.4}$$

With the measurement of RM at different wavelengths it is possible to have an estimation of the integral $\int_0^{l_s} n_e(l)B_{\parallel}(l)dl$. It turns out that the knowledge of the electron density along the line of sight n_e is necessary to infer the value of $B_{\parallel}$.

Observing galaxy clusters in X-ray it is possible to constrain n_e and thus to obtain $B_{//}$. The resulting values are $B \sim 0.2 - 3\mu$G (Taylor, Barton & Ge 1994).

For the IGMF measurement only theoretical models on the distribution of electrons in the universe can provide un upper limit on B_{IGMF}. Assuming that the electron distribution follows the Lyα forest distribution Blasi, Burles & Olinto (1999) found $B_{\mathrm{IGMF}} \sim 10^{-9}$G with a coherence lengths equal to the Hubble distance.

3.2.2 Constraints from CMB anisotropies

The presence of a magnetic field at the time of decoupling ($z_d \simeq 1100$) should have influence on the expansion of the Universe. Studying the angular spectrum of CMB can in principle give information on the cosmological magnetic field (Zel'dovic & Novikov 1983; Madsen 1989; Barrow, Ferreira & Silk 1997). Analizing the 4-years Cosmic Background Explorer (COBE) data, Barrow, Ferreira & Silk (1997) put the following constraint on the cosmic magnetic field:

$$B_{cos} < 5 \times 10^{-9} h_{75} \Omega^{1/2} \mathrm{G} \tag{3.2.5}$$

Taking into account the damping of magnetic field due to the photon diffusion and analyzing the COBE/FIRAS data, Jedamzik, Katalinic & Olinto (2000) derived a limit on the magnetic field strength of:

$$B_{cos} < 3 \times 10^{-8} \mathrm{G} \tag{3.2.6}$$

between comoving scales $\sim$ 400 pc and 0.6 Mpc.

3.2.3 Costraints from Big Bang Nucleosynthesis

Another indirect way to constrain the cosmological magnetic field comes from the Big Bang Nucleosynthesis (BBN) (Schramm & Turner 1998; Olive, Steigman & Walker 2000) that occurred between 10^{-2} and 1 s after the Big Bang. During this evolutionary phase electrons and protons recombine to produce the elements D, ^{4}He, ^{3}He and ^{7}Li. The presence of a non vanishing magnetic field during the nucleosynthesis can alter theoretical prediction on the abundances of elements. Thus, as there is tight agreement between theory and observation, the presence of magnetic field must not spoil the BBN prediction. According to this fact, it follows that the value of cosmic magnetic field at the present epoch should be:

$$B_{cos} < 10^{-6} \mathrm{G} \tag{3.2.7}$$

that is two order of magnitude larger that in eq.(3.2.6).

3.2.4 Constraints from γ-ray observations

The techniques described in the previous section provide upper limits on the IGMF. As pointed out before, different works have been carried out for deriving lower limits to IGMF based on the assumption that the suppression of the cascade emission is due to the fact that the size of the cascade source is much larger than the point spread function (psf) of *Fermi*-LAT. In the following we sum up the main feature and parameters of each work.

- *Neronov & Vovk (2010)* for the first time use *Fermi*-LAT data to costrain the IGMF. They analyzed four BL-Lac detected in TeV band with no emission in the GeV band with the Cherenkov telescope HESS. They obtain a $B_{\rm IGMF} > 3 \times 10^{-16}$G for the source 1ES 0229+200 with a coherence length of 1 Mpc. They reproduced the cascade with a Monte Carlo code assuming an isotropic emission and adopting the EBL model of Franceschini, Vaccari & Rodighiero (2008).

- *Tavecchio et al. (2010)*, analyzed the source 1ES 0229+200 assuming an emission angle $\theta_j = 0.1$ rad, an analytical cascade model limited at the first interaction and the EBL model of Kneiske et al. (2004) fitting the spectrum with a power low. They inferred a $B_{\rm IGMF} > 5 \times 10^{-15}$G. In a subsequent paper Tavecchio et al. (2011) re-analyzed 1ES 0229+200 fitting the H.E.S.S. data with a SSC model (see chapter 1) and taking into account also the second order in the cascade emission. They found $B_{\rm IGMF} > 2 \times 10^{-15}$G.

- *Dolag et al. (2011)* studied the source 1ES 0229+200 modeling the

emission spectrum with a broken power law, the cascade emission with a Monte Carlo code and assuming the EBL model of Kneiske & Dole 2010 they found $B_{\rm IGMF} > 5 \times 10^{-15}$G. For the first time they also take into account the suppression of the cascade due to the time delay of the secondary emission, finding a IGMF two order of magnitude lower than the previous.

Previous GeV/TeV inferences of the strength of the IGMF make an assumption that the mean blazar TeV flux over millions of years remains similar to values observed over the last few years. Here we take into account the time delay between direct and secondary emission. Fig. 3.1 sums up the bounds of IGMF derived with the techniques described in the previous sections. Note that lower bounds do not take into account our new limits based on time delay but are based on works of Neronov & Vovk (2010).

3.3 Time delay

As show before, γ-ray astrophysics provide a new technique to put a limit on the value of IGMF. In this section we show the basic idea of our model.
Consider a source and a observer separated by a distance d, as shown in Fig. 3.2. Photons with dimensionless energy $\epsilon_1 = h\nu_1/m_e c^2 \sim 2\times10^6 E_1({\rm TeV})$ emitted at angle θ_1 with respect to the line of sight between the source and observer, travel a mean distance $\lambda_{\gamma\gamma} = \lambda_{\gamma\gamma}(\epsilon_1, z)$ before converting into an electron-positron pair via $\gamma\gamma$ absorption with photons of the EBL. The pairs scatter CMB photons to $E_{\rm GeV}$ GeV energies, which are detected at an angle θ with respect to the line of sight to the source when the secondary electron and positrons (hereafter referred to as electrons) are deflected by an angle $\theta_{\rm dfl}$.

The GeV emission, in order to be detected, must be within the energy-dependent *Fermi*-LAT psf angle $\theta_{\rm psf}$. The system is treated in the low redshift limit (see Neronov & Semikoz 2009).

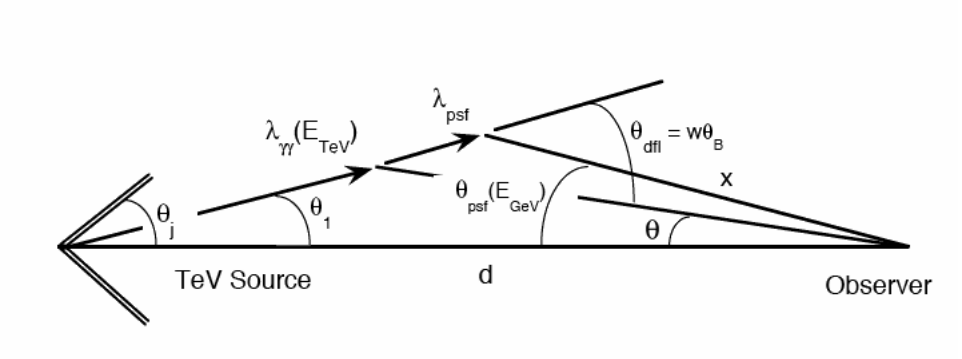

Figure 3.2: Sketch of the geometry of the process. A photon with energy $E_{\rm TeV}$ TeV, emitted at angle $\theta_1 \leq \theta_{\rm j}$ to the line of sight, interacts with an EBL photon to create an electron-positron pair with Lorentz factor $\gamma = 10^6\gamma_6$. The lepton is deflected through angle $\theta_{\rm dfl}$ and scatters a CMB photon to energy $E_{\rm GeV}$ GeV, which is observed as a source photon by the Fermi LAT if it is detected at an angle $\theta < \theta_{psf}(E_{\rm GeV})$ to the source. The underlying simplifying kinematic relation in the semi-analytic model is $\gamma_6 \approx E_{\rm TeV} \approx \sqrt{\rm E_{GeV}}$

The time delay Δt between the direct photons and the secondary formed by the process described above is given by:

$$c\Delta t = \lambda_{\gamma\gamma} + x - d \;\; = \;\; \lambda_{\gamma\gamma}\frac{d\sin(\theta_{\rm dfl})}{\sin\theta_{\rm dfl}} - d = \lambda_{\gamma\gamma}(1-\cos\theta_{\rm dfl}) - d(1-\cos\theta) \qquad (3.3.1)$$

where $x = d\sin\theta_1/\sin\theta_{\rm dfl}$ and $\lambda_{\gamma\gamma}$. In the limit of small observing and deflection angles, eq. (3.3.1) implies:

$$\Delta t \sim \frac{\lambda_{\gamma\gamma}}{2c}\theta_{\rm dfl}^2 \qquad (3.3.2)$$

provided that photon is detected at an angle:

$$\theta = \frac{\lambda_{\gamma\gamma}({\rm E_{TeV}})\theta_{\rm dfl}}{d} < \theta_{\rm psf}({\rm E_{GeV}}) \qquad (3.3.3)$$

to the source. Note that the deflection angle depends on either the primary photon energy $\rm E_{TeV}$ or Compton-scattered photon energy $\rm E_{GeV}$, since they

are related by $\mathrm{E_{GeV}} \sim \mathrm{E_{TeV}}$ as we now show.

The average CMB photon energy at low redshift is $\epsilon_0 \sim 1.24 \times 10^{-9}$ in $m_e c^2$ units, so that mean Thomson-scattered photon energy is $\epsilon_T \sim (4/3)\epsilon\gamma^2$ where $\gamma \sim E_{\rm TeV}/(2m_e c^2)$ implies $\gamma_6 = (\gamma/10^6) \simeq 0.98 E_{\rm TeV}$. Thus, an electron with Lorentz factor γ scatters CMB radiation to photon energy E when $\gamma_6 \cong E_{\rm TeV} \cong 1.1\sqrt{E_{\rm GeV}}$. The characteristic length scale for energy losses due to Thomson scattering is $\lambda_{\rm T} = 3m_e c^2/4\sigma_{\rm T} u_{\rm CMB}\gamma = (0.75/\gamma_6)$ Mpc, where $u_{\rm CMB} \cong 4 \times 10^{-13}$ erg cm^{-3} is the CMB energy density at low redshifts. While losing energy, the electron is deflected by an angle $\theta_{\rm B} \cong \lambda_{\rm T}/r_{\rm L}$ in a uniform magnetic field of strength $B_{\rm IGMF} = 10^{-15} B_{-15}$ G oriented perpendicular to the direction of motion of the electron, where the Larmor radius $r_{\rm L} = m_e c^2 \gamma/eB \cong 0.55(\gamma_6/B_{-15})$ Mpc. Thus, the deflection angle for an electron losing energy by scattering CMB photons to energy E in a uniform field is $\theta_B = \lambda_{\rm T}/r_{\rm L} \cong 1.1 B_{-15}/E_{\rm GeV}$. Introducing a coherence length λ_{coh}, then the deflection angle

$$\theta_{dfl} \equiv w\theta_{\rm B}; \;\; \text{with w} = \begin{cases} 1 & \text{if } \lambda_{\rm T} < \lambda_{\rm coh} \\ \\ \sqrt{\frac{\lambda_{coh}}{\lambda_{\rm T}}} & \text{if } \lambda_{\rm T} > \lambda_{\rm coh} \end{cases} \tag{3.3.4}$$

For 1ES 0229+200, photons has been detected to energies $E \lesssim 12$ TeV Aharonian et al. (2007), with an $\approx 15\%$ error in the energy measurement. An uncertainty in the analytic treatment comes from the fact that the mean free path $\lambda_{\gamma\gamma}(E_{\rm TeV})$ varies by a factor of ≈ 2 between $z = 0$ and $z = 0.14$, and it is different in different EBL models (see chapter 4). For instance, the EBL model of Finke Razzaque & Dermer (2010) gives $\lambda_{\gamma\gamma}(E) \cong 200$ Mpc, 125 Mpc, and 70 Mpc at $E = 1, 3$, and 10 TeV, respectively, and a low EBL model based on galaxy counts (Kneiske & Dole 2010) gives $\lambda_{\gamma\gamma}(E) \cong 280$ Mpc, 150 Mpc, and 85 Mpc, respectively.

For analytic estimates, we write $\lambda_{\gamma\gamma} = 100\lambda_{100}$ Mpc, though we use the

accurate energy dependence of $\lambda_{\gamma\gamma}(E_{\rm TeV})$ in the numerical calculations.

The importance of pair-cascade radiation with angular extent broader than the *Fermi*-LAT psf depends on the value of

$$\frac{\lambda_{psf}}{\lambda_{\gamma\gamma}} \cong \frac{d\theta_{psf}(E_{\rm GeV})/\theta_{dfl}}{\lambda_{\gamma\gamma}} \cong \frac{\tau_{\gamma\gamma}(E_{\rm TeV})\theta_{psf}(E_{\rm GeV})}{\theta_{dfl}} \tag{3.3.5}$$

where λ_{psf} is the effective distance a primary photon would have to travel to make a GeV photon detected at the edge of the *Fermi*-LAT psf given the parameters of the IGM. The value of $\theta_{psf}(E_{\rm GeV})$, taken here as the 95% *Fermi*-LAT confinement angle, is from the *Fermi*-LAT instrument performance page[1].

For the EBL model of Finke, Razzaque & Dermer (2010), the cascade emission can be treated as a point source when $B/10^{-15}{\rm G} \ll 0.05{\rm E}_{\rm GeV}^{0.6}$ for $0.2 \lesssim E_{\rm GeV} \lesssim 20$. For a source at distance $d = d_{\rm Gpc}$ Gpc, with $d_{\rm Gpc} \sim 1$ corresponding to $z \sim 0.2$, the time delay for emission observed at angle

$$\theta \cong 0.01\ \frac{\lambda_{100}}{d_{\rm Gpc}}\ \big(\frac{B_{-15}w}{E/10\ {\rm GeV}}\big) \tag{3.3.6}$$

from the line of sight is given from eq. (3.3.2) by

$$\Delta t({\rm yr}) \cong 2\times 10^6\ \lambda_{100}\big(\frac{B_{-15}w}{E/10\ {\rm GeV}}\big)^2 \tag{3.3.7}$$

Short delay times are restricted to conditions of small $B_{\rm IGMF}$ and large E where, as just seen, extended pair halo emission can be neglected.

Eq. (3.3.7) shows that small time delays are implied when $\lambda_{\gamma\gamma}$ is small and $\lambda_{psf}/\lambda_{\gamma\gamma} > 1$. When $\lambda_{\gamma\gamma} \lesssim \lambda_{\rm T}$, an additional delay $\approx \lambda_{\rm T}\theta_{\rm dfl}^2/c$ arises during the time that the electrons are losing energy and being deflected by the IGMF. Such small values of $\lambda_{\gamma\gamma} \sim 1$ Mpc are only relevant at low redshifts for $\gtrsim 100$ TeV photons that pair-produce within ≈ 1 Mpc of their source, where the magnetic field may not be representative of the dominant volume of the voids.

[1] www-glast.slac.stanford.edu/software/IS/glast_lat_performance.htm

3.4 γ-ray data of 1ES 0229+200

The TeV blazar 1ES 0229+200, which provides some of the strongest constraints on the lower limit to the IGMF, was observed with HESS (Aharonian et al. 2007) in 2005 and 2006 and with VERITAS (Perkins et al. 2010) in October 2009 – January 2010.

No evidence for variability of the TeV flux has been reported, so the observations give an average TeV flux from this source on timescales of ≈ 3 yr, though with poor sampling. The HESS and preliminary VERITAS data (Perkins et al. 2010) are shown in Fig.(2.3, 2.4, 2.5) by the blue open circles and red squares, respectively. *Fermi*-LAT upper limits on TeV blazars were reported previously (Abdo et al. 2009; 2010). Here we reanalyze the *Fermi*-LAT data for 1ES 0229+200 collected from 2008 August 4 to 2010 September 5 in survey mode. To minimize systematics, only photons with energies greater than 100 MeV were considered in this analysis. In order to avoid contamination from Earth-limb γ rays, a selection on events with zenith angle $< 105^\circ$ was applied (Atwood et al. 2009). This analysis was performed using the standard likelihood analysis tools that are part of the Fermi ScienceTools software package (version v9r15p5).[2] The P6_V3_DIFFUSE set of instrument response functions was used. Photons were selected in a circular region of interest (ROI) 10° in radius, centered at the position of 1ES 0229+200. The isotropic background, including the sum of residual instrumental background and extragalactic diffuse γ-ray background, was modeled by fitting this component at high galactic latitude (isotropic_iem_v02.txt, available from the FSSC website). The Galactic diffuse emission model version "gll_iem_v02.fit," was used in the analysis. The profile likelihood method was used to extract 95% confidence level upper limits at the location of 1ES0229+200 assuming a power-law energy distribution with photon index=2, all 1FGL point sources lying within the ROI being modeled with power-law distributions. The up-

[2] http://fermi.gsfc.nasa.gov/ssc/.

per limits shown in Figure 2 are obtained in the energy bins 0.1 – 1 GeV, 1 – 3 GeV, 3 – 10 GeV, 1 – 10 GeV, and 10 – 100 GeV.

3.5 Model for cascade radiation

The computation of cascade emission produced by γ-ray photons interacting with EBL has been addressed in different works. Monte Carlo calculation have been computed by Aharonian et al. (1994), Plaga (1995), Coppi & Aharonian (1996), d'Avezac et al. (2007), Murase et al. (2008), Neronov & Semikoz (2009), Elyiv, Neronov & Semikoz (2009), Dolag et al. (2009), while analytical calculation by Bonometto & Rees (1970), Tavecchio et al. (2010; 2011).

Here we show our semi-analytical model for the cascade radiation spectrum. Let $\Phi = L_\star/4\pi d_L^2$ be the energy flux of a source with luminosity $L_\star$ at a distance d_L, thus $f_\epsilon = \nu F_\nu = \epsilon_\star L_\star/4\pi d_L^2$ where $\epsilon_\star = (1+z)\epsilon$.

The photons coming from the source at redshift z are absorbed so we have:

$$f_\epsilon = \frac{\epsilon_\star L_\star(\epsilon_\star)}{4\pi d_L^2}\exp(-\tau_{\gamma\gamma}(\epsilon)) \tag{3.5.1}$$

Assuming the low-redshift approximation (z$<<$ 1, $\epsilon_\star \simeq \epsilon$) and introducing the photon injection function of source $\dot{N}(t)$ we have:

$$\epsilon L_\epsilon = m_e c^2 \epsilon^2 \dot{N}(t) \tag{3.5.2}$$

The rate of surviving photons, after the interaction with EBL is $\dot{N}(t)\exp(-\tau_{\gamma\gamma}(\epsilon, \mathrm{z}))$ and thus the rate of absorbed photons is:

$$\dot{N}_{abs}(t) = \dot{N}(t)[1 - \exp(-\tau_{\gamma\gamma}(\epsilon, \mathrm{z}))] \tag{3.5.3}$$

Here $\dot{N}_{abs}$ represents also the electron injection function. As each photon makes two leptons and the energy of the leptons is $\gamma_i \simeq \epsilon/2$, so we have

$$\dot{N}_{inj}(t) = 4\dot{N}_{abs}(t) = 4\dot{N}(t)[1 - \exp(-\tau_{\gamma\gamma}(\epsilon, \mathrm{z})] \tag{3.5.4}$$

Thus we can rewrite eq.(3.5.1) as:

$$f_\epsilon = \frac{m_e c^2 \epsilon^2 \dot{N}(t)}{4\pi d_L^2} \exp(-\tau_{\gamma\gamma}(\epsilon, \mathrm{z}))] \tag{3.5.5}$$

and obtain the electron injection source as:

$$\dot{N}_{inj}(\gamma_i) = \frac{16\pi d_L^2}{m_e c^2 \epsilon^2} f_\epsilon [\exp(\tau_{\gamma\gamma}(\mathrm{t}, \mathrm{z})) - 1] \tag{3.5.6}$$

In Thomson regime, the energy loss rate for electrons is:

$$-\dot{\gamma} = -\frac{d\gamma}{dt} = \frac{4c\sigma_T u_0 \gamma^2}{3} \tag{3.5.7}$$

where σ_T is the Thomson cross section and $u_0 = u_{CMB}/m_e c^2$.

Defining $\nu_T = 4/3c\sigma_T u_0$, the solution to electron continuity equation is:

$$N(\gamma) = \frac{1}{\nu_T \gamma^2} \int_\gamma^\infty d\gamma' \dot{N}(\gamma') \tag{3.5.8}$$

Luminosity spectrum from Compton scattering in Thomson regime is (see e.g. eq. 6.68 in Dermer & Menon 2008):

$$\epsilon_s L_T(\epsilon_s) = \frac{3}{4} c\sigma_T u_{CMB} (\frac{\epsilon_s}{\epsilon_0})^2 \int_{\sqrt{(\epsilon_s/4\epsilon_0)}}^\infty d\gamma \frac{N_e(\gamma)}{\gamma^2} F_T(\tilde{\epsilon}) \tag{3.5.9}$$

where $F_T(\epsilon)$ represent the isotropic Thomson scattering kernel defined in the following manner:

$$F_T(\tilde{\epsilon}) = \frac{2}{3}(1 - \tilde{\epsilon}) \tag{3.5.10}$$

with $\tilde{\epsilon} = \epsilon_S/(4\gamma^2\epsilon_0)$.

Inserting eq. (3.5.6) in eq. (3.5.8) we have:

$$N_e = \frac{16\pi d_L^2}{\nu_T \gamma^2 m_e c^2} \int_\gamma^\infty d\gamma_i \frac{f_\epsilon [\exp(\tau_{\gamma\gamma}(\mathrm{t}, \mathrm{z})) - 1]}{\epsilon^2} \tag{3.5.11}$$

Substituting N_e into expression eq. (3.5.9) gives:

$$\epsilon_S L_T(\epsilon_S) = \frac{12\pi d_L^2 c\sigma_T u_0}{\nu_T} (\frac{\epsilon_S}{\epsilon_0})^2 \int_{\sqrt{(\epsilon_s/4\epsilon_0)}}^\infty d\gamma \quad \frac{F_T(\epsilon)}{\gamma^4} \times \int_\gamma^\infty d\gamma_i \frac{f_\epsilon [\exp(\tau_{\gamma\gamma}(\mathrm{t}, \mathrm{z})) - 1]}{\epsilon^2} \tag{3.5.12}$$

Table 3.1: Derived Limits on $B_{\rm IGMF}$ for the source 1ES 0229+200

1ES 0229+200	$\theta_{\rm j}$ (rad)	$B_{\rm IGMF}$(G)
Neronov & Vovk (2010)	π	$\gtrsim 3\times10^{-16}$
Tavecchio et al. (2010)	0.1	$\gtrsim 5\times10^{-15}$
Tavecchio et al. (2011)	0.03	$\gtrsim 2\times10^{-15}$
Dolag et al. (2011)	0.1	$\gtrsim 5\times10^{-15}$

Inserting the isotropic Thomson kernel (eq. 3.5.10) in eq. (3.5.12) and recolling that $\nu_T = 4/3c\sigma_T u_0$ finally we get:

$$f_{es} = \frac{3}{2}(\frac{\epsilon_S}{\epsilon_0})^2 \int^{\infty} d\gamma\gamma^{-4}(1-\frac{\epsilon_S}{4\gamma^2\epsilon_0}) \int_{\gamma}^{\infty} d\gamma_i \frac{f_\epsilon[\exp(\tau_{\gamma\gamma}(\mathrm{t},\mathrm{z}))-1]}{\epsilon^2} \quad (3.5.13)$$

Eq. (3.5.13) employs the isotropic Thomson kernel and using the Klein Nishina kernel makes negligible difference for photons with energy < 20 TeV. In the three terms in the lower limit of the external integration, the first gives the kinematic minimum electron Lorentz factor to scatter a CMB photon to energy ϵ_s. The second is the value of the deflection Lorentz factor $\gamma_{\rm dfl}$ obtained by equating the Thomson cooling time and the timescale $\theta_{\rm j} r_{\rm L}/c$ when the electron is deflected outside the photon beam of opening angle $\theta_{\rm j}$. The third limit, $\gamma(\Delta t_{eng})$, represents the Lorentz factor to which electrons have cooled after the blazar engine has been operating for time Δt_{eng}, and follows from eq. (3.3.2) by solving $\Delta t(\gamma_{eng}) < \Delta t_{eng}$ for $\gamma_{eng} = \gamma(\Delta t_{eng})$. Here we approximate $\lambda_{\gamma\gamma}(E_{\rm TeV}) \approx d\tau_{\gamma\gamma}(E_{\rm TeV})$ Mpc, using a fit to the Finke Razzaque & Dermer (2010) EBL model for 1ES 0229+200. A calculation with $\lambda_{\gamma\gamma}(E_{\rm TeV}) \approx d(2\tau_{\gamma\gamma}(E_{\rm TeV}))$ Mpc gives similar results. Only the first generation of cascade emission attenuated by the factor $\exp[-\tau_{\gamma\gamma}(\epsilon_1, z)]$ is shown here.

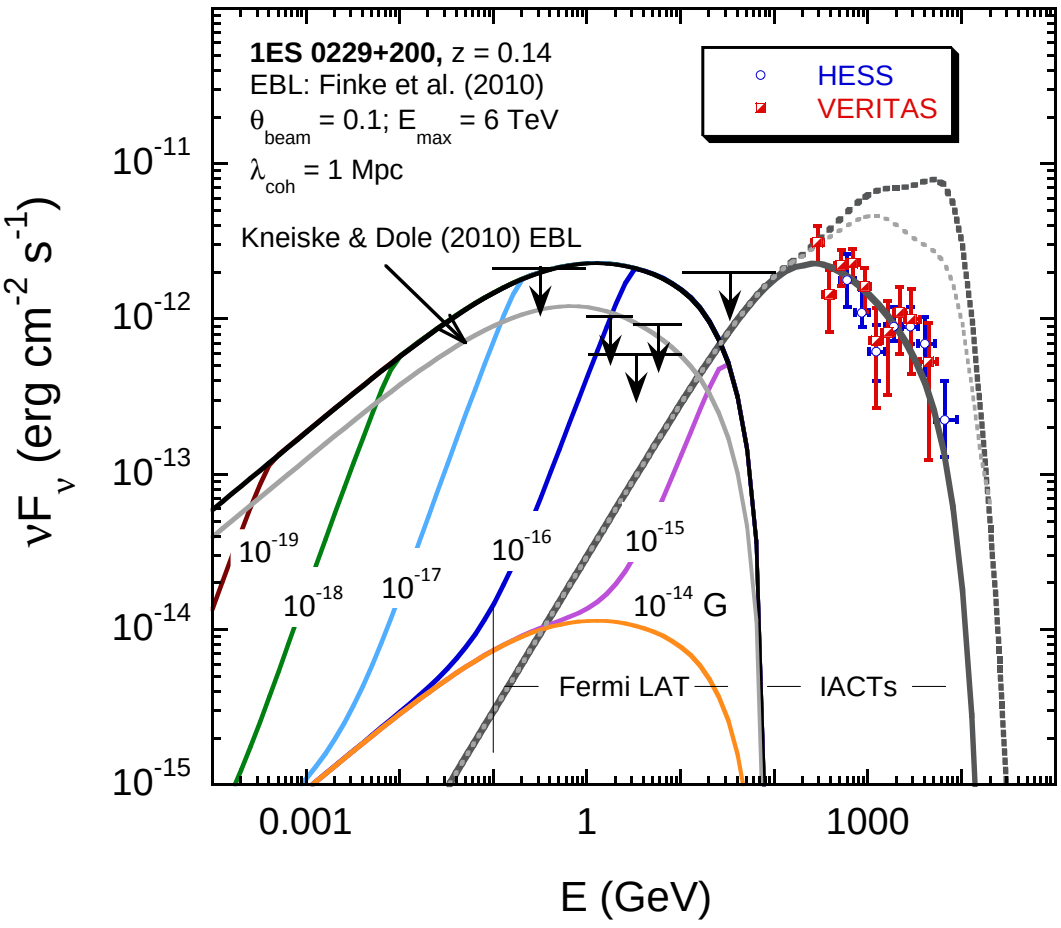

Figure 3.3: Model of cascade radiation spectrum, equation (3.5.13), applied to HESS, VERITAS, and *Fermi* observations of 1ES 0229+200, using model spectra (solid curves) and EBL model of Finke et al. 2010 to give attenuated source spectrum (dotted curves). Cascade spectra for 1ES 0229+200 assuming persistent TeV emission at the level observed with HESS and VERITAS, for different values of $B_{\rm IGMF}$ and $\lambda_{coh} = 1$ Mpc (solid) or $\lambda_{coh} = 100$ kp (dot-dashed). The psf constraint for the $\lambda_{coh} = 1$ Mpc case is shown by the dashed curves.

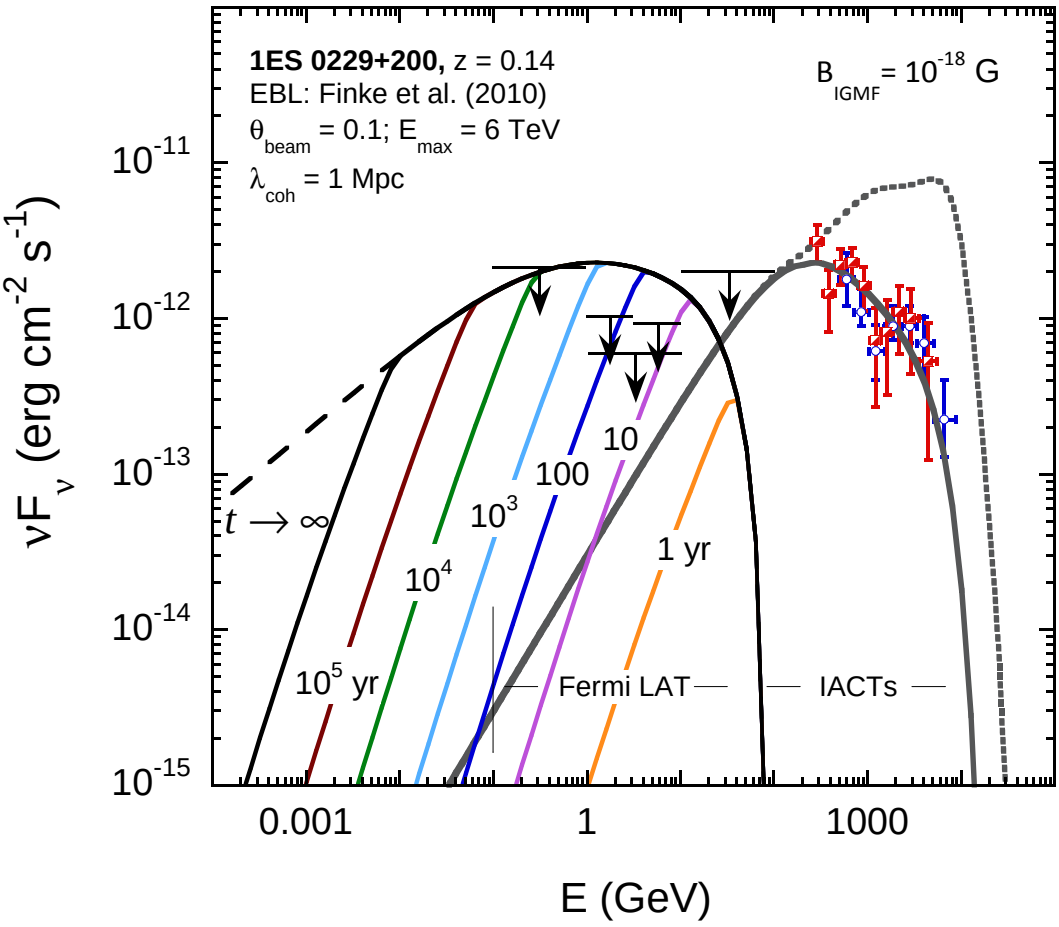

Figure 3.4: The Figure shows the cascade spectra when source radiates TeV flux for 3 yr with constant average spectrum given by power-law with νF_ν index $= 4/5$ for source spectrum with superexponential cutoff $\propto \exp[-(E/5\ \mathrm{TeV})^2]$ are shown for the case $\lambda_{coh} = 1$ Mpc with different values of B_{IGMF}, as labeled.

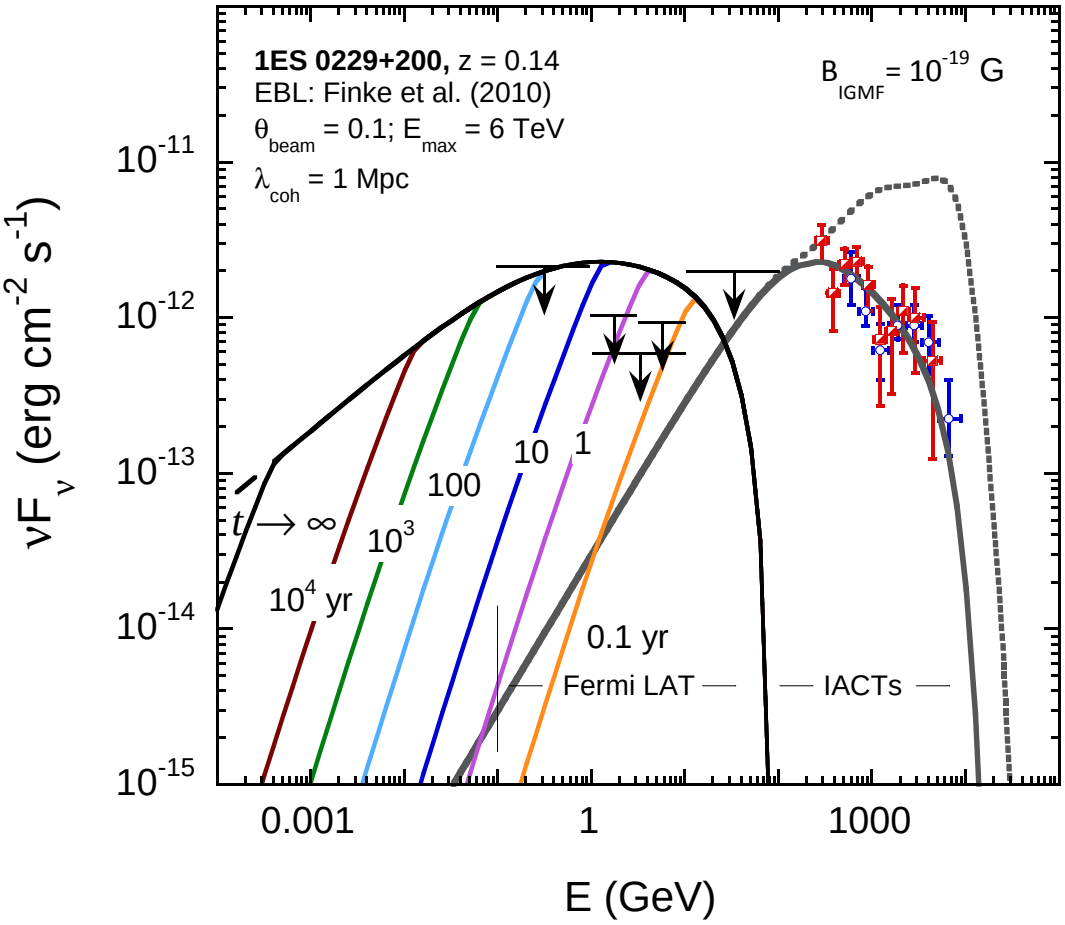

Figure 3.5: The Figure shows the cascade spectra when source radiates TeV flux for 3 yr with constant average spectrum given by power-law with νF_ν index $= 4/5$ for source spectrum with exponential cut off $\propto \exp[-(E/10\ \mathrm{TeV})]$ are shown for the case $\lambda_{coh} = 1$ Mpc with different values of B_{IGMF}, as labeled.

3.6 Results

Results of calculations using the simplified analytic model are shown in Fig. 3.3 and Fig. 3.4, is a calculation where the blazar engine operates for indefinitely long times, with the reduction of cascade flux due to deflection away from the beam for a jet and the detection of a plateau flux of isotropized radiation determined by the jet opening angle $\theta_{\rm j} = 0.1$ (Tavecchio et al. 2010). The source spectrum is described by a super-exponential cutoff power law $\nu F_\nu \propto E^{4/5} \exp[-(E/5\ {\rm TeV})^2]$ in Figs. 3.3 and 3.4, and by an exponential cutoff power law $\nu F_\nu \propto E^{4/5} \exp(-E/10\ {\rm TeV})$ in Fig. 3.5.

In agreement with previous results (Neronov & Vovk 2010; Tavecchio et al. 2010; Tavecchio et al 2011; Dolag et al. 2011), a value of $B_{\rm IGMF} \gtrsim 3 \times 10^{-16}$ G is needed in order to reduce the GeV flux below the *Fermi* upper limit.

From the calculations, we also find that under the assumption of persistent TeV blazar emission, halo emission becomes increasingly dominant for large jet opening angles. Detection of halos around AGNs, as claimed by Ando & Kusenko (2010) (but see Neronov et al. 2011), would then favor detection in sources with large opening angle, long lived TeV engines. Also under the persistent emission hypothesis, a maximum jet opening angle $\theta_{\rm j} \lesssim 0.4$ is implied in order that the isotropized radiation does not violate the *Fermi*-LAT upper limits.

The effects of $B_{\rm IGMF}$ on the received spectrum of reprocessed TeV radiation when the blazar engine is assumed to emit a constant TeV flux over an engine time $\Delta t_{eng} \cong 3$ yr are shown in Figs. 3.3 and 3.4.

These calculations show that $B_{\rm IGMF} \gtrsim 3 \times 10^{-19}$ G for the case where the assumed source spectrum is sharply cut off above 5 TeV. Uncertainties in the analytic model, including the strong sensitivity of the cascade spectrum on γ_{eng}, relaxes our conclusions to an analytic, order-of-magnitude minimum IGMF of $B_{\rm IGMF} \gtrsim 10^{-18}$ G for $\Delta t_{eng} \cong 3$ yr. Fig. 3.5 shows that the minimum magnetic field also depends sensitively on the characterization of the

high-energy spectral flux, which can then quickly cascade into the 10 – 100 GeV band and violate one of the *Fermi* upper limits (or detection; see Orr et al. 2011). By assuming source spectra with larger fluxes above ≈ 5 – 10 TeV, Dolag et al. (2011) and Tavecchio et al. (2011), derive larger values for the minimum $B_{\rm IGMF}$, but not more than a factor of a few above the analytic results when difference in activity times and primary source fluxes are considered.

Our knowledge of the blazar engine is not deep enough as to have high confidence in this assumption, though some models for slowly varying TeV flux from TeV blazars can be noted. For example, a slow cooling rate of the electrons that produce the TeV photons could imply a slowly varying γ-ray flux even if the blazar engine is very active.

For electrons scattering photons to TeV energies, the synchrotron cooling time in the observer frame is $t_{syn} \cong (1+z)6\pi m_e c/(\delta_{\rm D}\sigma_{\rm T}B'^2\gamma') \cong 50/E({\rm TeV})$ yr, using the fitting parameters of Tavecchio et al. 2010 for 1ES 0229+200 (break Lorentz factor $\gamma_{br} = 5\times10^6$, emission region magnetic field $B' = 5\times10^{-4}$ G, and Doppler factor $\delta_{\rm D} = 40$). Relativistic electrons in an extended jet that Compton scatter photons of the CMB could also make slowly varying TeV radiation in sources like 1ES 0229+200 or 1ES 1101-232 (Böttcher, Dermer & Finke 2008). In this model, relativistic electrons lose energy on timescales of $\approx 750/[(\Gamma/10)^2\sqrt{E({\rm TeV})}$ yr. These models do not, however, provide good reasons to expect TeV blazars to produce steady flux for thousands or millions of years. A more reliable limit is obtained from direct measurements of TeV fluxes. For the handful of observations of 1ES 0229+200 over 3 – 4 years of observing (Aharonian et al. 2007; Perkins et al. 2010), no TeV flux variations have been reported. Using such timescales leads to a limit of

$$B_{\rm IGMF}({\rm G}) \gtrsim 10^{-18}({\rm E/10\ GeV})\sqrt{\Delta {\rm t}/3\ {\rm yr}}\sqrt{\lambda_{100}}, \qquad (3.6.1)$$

assuming that $\lambda_{coh} \approx 1$ Mpc. By assuming strong intrinsic $\gtrsim 10$ TeV emission from 1ES 0229+200 (which is not observed because of EBL attenuation),

Fermi LAT flux upper limits at ≈ 100 GeV can be violated, leading to larger limiting values of $B_{\rm IGMF}({\rm G}) \gtrsim 5 \times 10^{-18}$ G. Evidence for a strong primary flux at $\gtrsim 10$ TeV comes from detection of a shoulder feature at ≈ 1 TeV, as found in the numerical calculations of Dolag et al. (2011) and analytical results (Fig. 3.5), and suggested by the joint VERITAS/HESS data. Note that our calculations assume negligible contribution from cascades induced by photopair interactions by $\gtrsim 10^{18}$ eV cosmic rays (Essey et al. 2010).

3.7 Conclusions

In this work we have highlighted the importance of the time delay between direct and secondary photons when the suppression of cascade emission is taken into account. We find a lower limit for IGMF $B_{\rm IGMF} \gtrsim 10^{-18}$G assuming the source activity of 3-4 yrs.

Recently Taylor, Vovk & Neronov (2011) have studied in details the time delay of of 1ES 0229+200 by a Monte Carlo calculation finding $B_{\rm IGMF} \sim 10^{-17}$ G for a $\tau \sim 1yr$ that is in agrement with our result.

More frequent, sensitive, and broadband GeV – TeV observations of 1ES 0229+200 can test whether the average TeV flux corresponds to the flux that has been historically measured or is unusual. Evidence for long-lived TeV radiation can be found in pair halos (Aharonian et al. 1994) from misaligned blazar candidates such as Cen A or M87.

A large field-of-view detector like the High Altitude Water Cherenkov telescope (Goodman 2010), or systematic monitoring campaigns of blazars like 1ES 0229+200 (z = 0.14), 1ES 1101-232 (z = 0.186), 1ES 0347-121 (z = 0.185) or other bright, moderate redshift BL Lacs with the present generation of air Cherenkov telescopes or an advanced Cherenkov telescope array, will give better information about the duty cycle of TeV blazars and could provide more secure constraints on the value of the intergalactic magnetic field.

Chapter 4

Extragalactic Background Light

4.1 Introduction

In the previous chapters we have shown how γ-ray photons are absorbed by the so called EBL and how important is its role in affecting blazar spectra. With the term EBL we refer to the integrated light emitted by galaxies, quasars and dust during the universe history, from UV to far infrared (FIR) wavelengths ($\sim$ 0.1-1000μm). The spectral energy distribution of redshifted radiation is characterized by a two bumps shape (see Fig. 4.3). The first peak of $\sim$ 1 μm is due to radiation emitted by stars in galaxies, while the second peak around 100 μm is produced by starlight absorbed and re-emitted by dust.

Because of foreground contaminations due mainly to zodiacal light, direct observations of the EBL are difficult. Reliable lower limits come from galaxy counts performed with the *Hubble Space Telescope* (HST), (Madau & Pozzetti 2000) and *Spitzer* telescope (Fazio et al. 2004)

High energy astrophysics provide another way to constrain the EBL: blazar spectra are modified by the interaction with EBL photons producing electron/positron pairs (Gould & Schreder 1967). The pair production cross

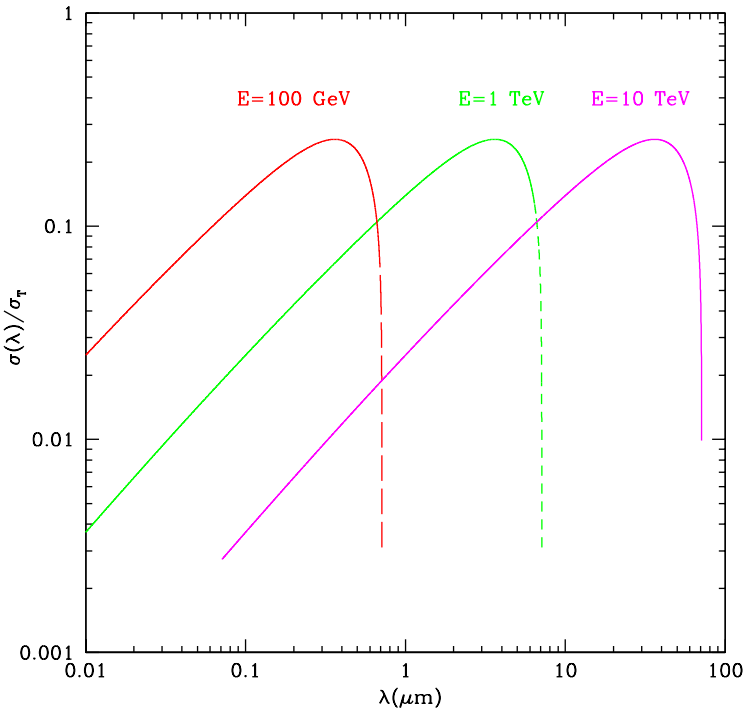

Figure 4.1: The pair production cross integrated cross section for different incoming photon energy.

section peaks sharply at:

$$\lambda = 2.4 \left(\frac{E_\gamma}{\mathrm{TeV}} \right) (\mu\mathrm{m}) \tag{4.1.1}$$

where E_γ is the γ-ray photon energy. Thus 10 TeV γ-ray can probe the far IR band (FIR), 1 TeV photons the mid IR (MIR) and 100 GeV the near IR (NIR) part of EBL (Fig.4.1)

Stecker et al. (1992) in a pioneering work made use of this phenomenon for the blazar 3C 279: assuming an intrinsic γ-ray spectrum for 3C 279, the observed absorbed spectrum, gives is in principle information about the EBL. Although intrinsic γ-ray spectrum is poorly known, the method allow us to put upper limits on the EBL.

From the theoretical point of view, in the last three years several new EBL models have been proposed and applied to the increasing number of blazar

spectra detected with *Fermi*-LAT and Cherenkov telescopes. Theoretical models can be collected in three classes. In the so called *backwards* evolution models, cosmological observable parameters are extrapolated at different redshifts to obtain the luminosity density (Stecker Malkan & Scully 2006; Franceschini, Rodighiero & Vaccari 2008). In the *forward* models, the cosmic star-formation is computed starting from merger-tree models of galaxies formation and convolved with synthetic galaxy SED to obtain the EBL (Primack et al. 2005; Gilmore et al. 2010). Finally in the so-called *semi-empirical* models, the observational cosmic star-formation rate is convolved with synthetic models for stellar emission in galaxies to infer the EBL at different redshifts (Kneiske et al. 2002, 2004; Kneiske & Dole 2010; Finke, Razzaque & Dermer 2010). Here, after a brief review of direct and indirect observations (section 4.2) and a description of theoretical models (section 4.3) we present our semi-empirical model to describe the EBL at different redshift (section 4.4). Conclusions will be given in section 4.5.

4.2 Observations and measurements

As pointed before, direct measurements of the EBL are difficult because of the presence of foreground emission mainly due to zodiacal light that is approximately up to three order of magnitude more intense than genuine EBL component, as shown in Fig4.2. Once zodiacal light is subtracted, the Milky Way emission dominates over EBL in the optical and NIR band while CMB in the FIR band. Nevertheless recent direct measurement of EBL exist and are:

- optical measurements with the *Hubble Space Telescope* by Bernstein (2007).
- COBE/DIRBE data from 1.25 to 2.2 μm (Cambresy et al. 2001);
- data from IRTS between 2.2 and 4 μm (Matsumoto et al. 2005);

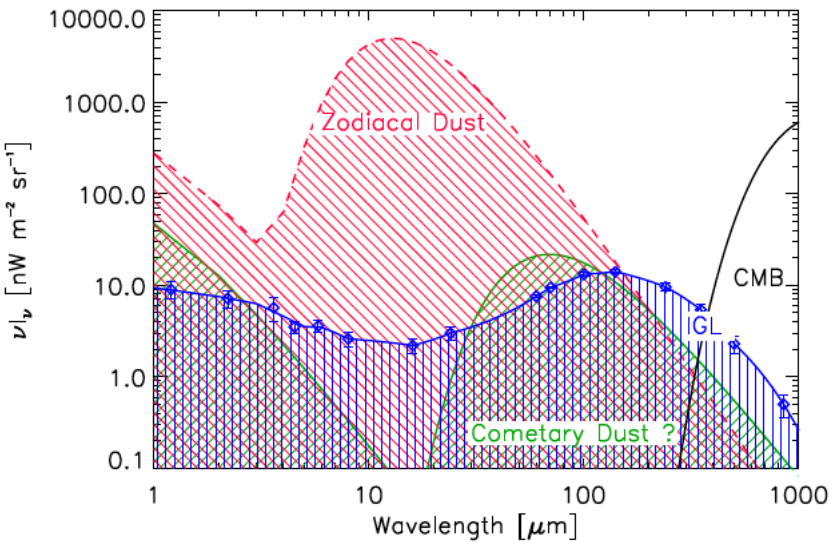

Figure 4.2: Comparison between zodiacal light (red region) and integrated galaxies light (blue region) from Chary & Pope (2010).

- Spitzer measurement at 3.6 μm (Levenson & Wright 2008);
- COBE/FIRAS data at 125 μm (Lagache et al. 2008);
- ISO data at 170 μm (Juvela et al. 2009)

Indirect measurements allow to put either lower and upper limits on the value of EBL. A way to put a lower limit has been developed by Madau & Pozzetti (2000) counting the galaxies detected by the *Hubble Space Telescope* in the optical band and by *Spitzer* (Fazio et al. 2004) in the near infrared (NIR). With this technique, analyzing data from *Spitzer*, Bethermin et al. (2010) gave a robust estimation of the galaxy contribution to the so called Cosmic Infrared Background (CIB).

Upper limits to EBL can be put in principle using blazar spectra. This idea has been proposed in 1970 by Fazio & Stecker but only recently with the availability of Cherenkov telescopes (e.g. HESS, MAGIC, VERITAS) and new γ-ray satellites (*Fermi*-LAT and *AGILE*) has become feasible.

Blazar spectra show absorption features at γ-ray energies due to the interaction with the EBL (see section 4.4). Thus the relation between the blazar flux on Earth F_{obs} and the intrinsic blazar flux F_{int} emitted at redshift z is:

$$F_{int} = F_{obs} e^{\tau} \tag{4.2.1}$$

where τ is the $\gamma\gamma$ pair production optical depth (see eq.4.4.17) strongly dependent on the EBL. Assuming a power law SED for the blazar spectra in the γ-ray band (see chapter 2) with $\mathrm{d}N/\mathrm{dE} \propto \mathrm{E}^{-\Gamma_{\mathrm{int}}}$ with photon index Γ, eq.4.2.2 become:

$$E^{-\Gamma_{int}} = E^{-\Gamma'} e^{\tau} \tag{4.2.2}$$

where Γ' is the photon index measured on Earth. Assuming a theoretical maximum value for Γ_{int}, an estimation of τ and thus on EBL is possible. Aharonian et al. (2006) employed this technique with two blazars H2356-309 and 1ES 1101-232 detected at TeV energies by HESS. They assume a theoretical maximum spectral index $\Gamma_{int} \geq 1.5$ putting an upper limit on NIR band. Mazin & Raue (2007) analized a large number of TeV blazar posing new upper limits on EBL. The detection of blazars with *Fermi*-LAT in an energy band (20 MeV-300 GeV) where the absorption is negligible has allowed an improvement of this method. Basically, combining *Fermi*-LAT and Cherenkov telescope observations it is possible to obtain the intrinsic spectral index Γ_{int}, thus constrain the EBL. The underlying assumption is that blazars have the same power law index in the GeV and TeV bands. Using this method Gearganopoulos, Finke & Reyes (2010) exclude the validity of the EBL model of Stecker Malkan & Scully (2006) also excluded by Orr, Krennrich & Dwek (2011) with a similar method. The *Fermi* group provided an accurate analysis of all blazars with redshift up to z=3 to constrain theoretical EBL models. They exclude at high level the model of Stecker Malkan & Scully (2006) as is shown in Fig. 4.4

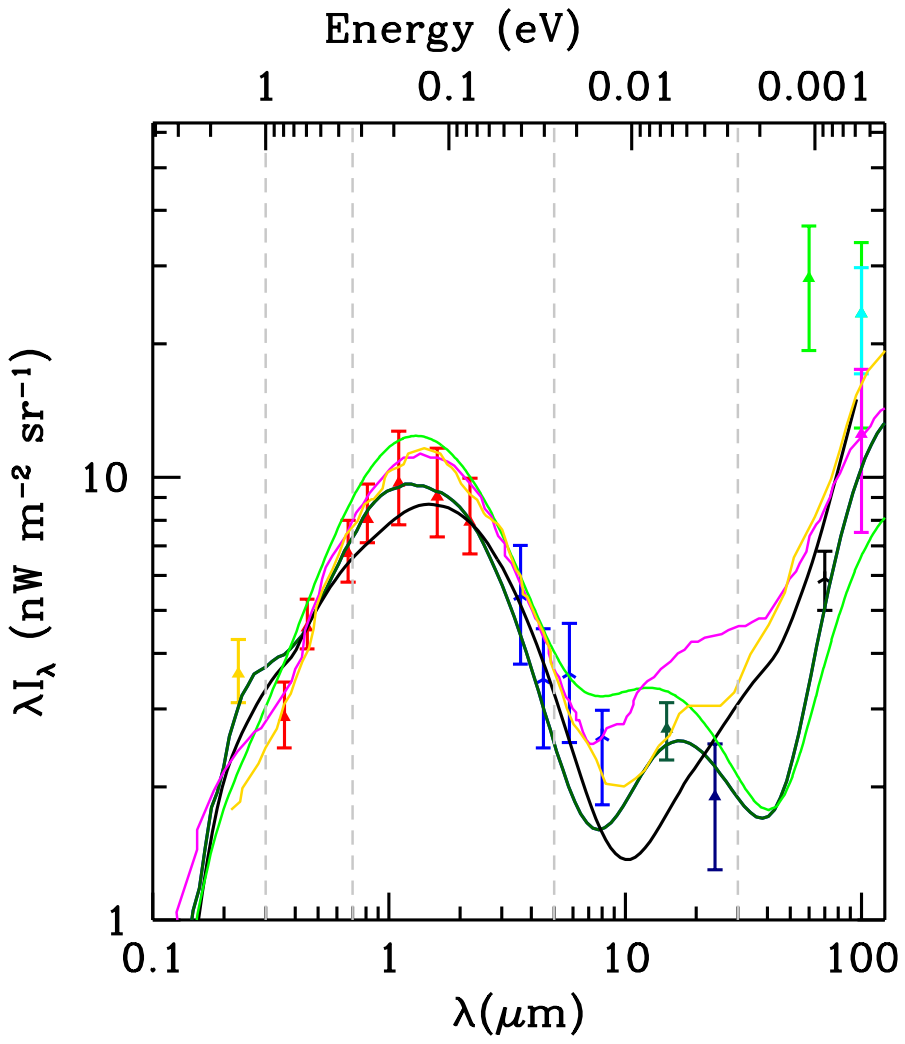

Figure 4.3: Different EBL models, Franceschini et al. (2008) (gold line), Gilmore et al. (2010) (magenta line), Kneiske & Dole (2010) (dark green line), Finke et al. (2010) (light green line) and our model (black line) with lower limits and observations by Madau & Pozzetti (2000) (red points), Fazio et al. (2004) (blue points), Metcalfe et al. (2003) (dark green point), Chary et al. (2004) (dark blue point), Frayer et al. (2006) (black point), Wright et al. (2004) (magenta points), Lagache et al. (2000) (cyan point), Finkbeiner et al. (2000) (green point). Dotted grey line separate the different energy band: UV, optical, NIR, MIR and FIR band.

4.3 Theoretical Models

As shown in the section 4.1 theoretical studies of the EBL have experienced a rapid growth in the last three years. In this section we show the most significant and complete models. Theoretical models must reproduce the local (z=0) observations (see section 4.2) and must describe the evolution of different components of EBL at different redshifts. This implies assumptions on how galaxies and quasars evolve, and how dust absorbs and re-emits the UV-optical radiation. In other words, one needs to know the galaxy and quasar luminosity function at different redshifts or the cosmic star-formation history and convolve it with different galaxy and quasar spectra. Distinct models present different ways to compute these cosmological parameters with different degrees of complexity.
In the next paragraphs we follow the classification proposed by Hauser & Dwek (2001).

- *semi-empirical models*: the first model of this kind was made by Kneiske et al. (2002), updated in 2004. The basic idea is to convolve the synthetic SED of galaxies computed by Bruzual & Charlot (1998) with a parametric fit of the cosmological star-formation history to obtain the comoving emissivity. Galaxy SEDs are constructed by using population synthesis models (see Bruzual & Charlot 1998; 2003) and are computed for different star-formation rate, initial mass function (IMF) and chemical evolution. The EBL is then obtained integrating the comoving emissivity over the redshift.

  Finke, Razzaque & Dermer (2010) performed a similar calculation using analytic expression for radiation from stars and dust re-emission. No metallicity evolution has been taken into account. In all these models specific dust extinction laws and dust emission are adjusted to match observations.

- *forward evolution models*: models belonging to this class are charac-

terized by the use of semi-analytic models (SAMs) of galaxy formation to predict the EBL. The most recent model of this kind (Gilmore et al. 2010) is based on the SAM described in Somerville & Primack (1999) and Somerville, Primack & Faber (2001). The galaxy evolution is computed by merger trees of DM halo constructed via Monte Carlo techniques based on the Extendend Press-Schecter theory. The star-formation and chemical enrichment history for each galaxies are convolved with synthetic SEDs computed by Bruzual & Charlot (2003) assuming a Chabrier IMF. The model takes into account the reprocessing of ionizing radiation by the intergalactic medium (IGM) using the radiative transfer code CUBA (Haardt & Madau 1996; 2011).

- *backward evolution models*: These models extrapolate the spectral properties of local galaxies to higher redshifts using some parametric form for their evolution (Hauser & Dwek 2001). Stecker Malkan & Scully (2006) produced one of the first although the most representative model of this class has been build up by Franceschini, Rodighero & Vaccari in 2008. They analyzed a large amount of cosmological survey data from optical to FIR band, and compute number counts, redshift distributions and luminosity functions for different galaxy populations: early, late type galaxies and starburst galaxies. Being based on solid and complete observations, this model is considered the most reliable observationally-based EBL.

Finally a new model that does not belong to the previous class has been proposed by Dominguez et al. (2011) in which galaxy evolution is inferred from the observed evolution of the rest-frame K-band galaxy luminosity function up to redshift 4 (Cirasuolo et al. 2010), combined with a determination of galaxy SED-type fractions.

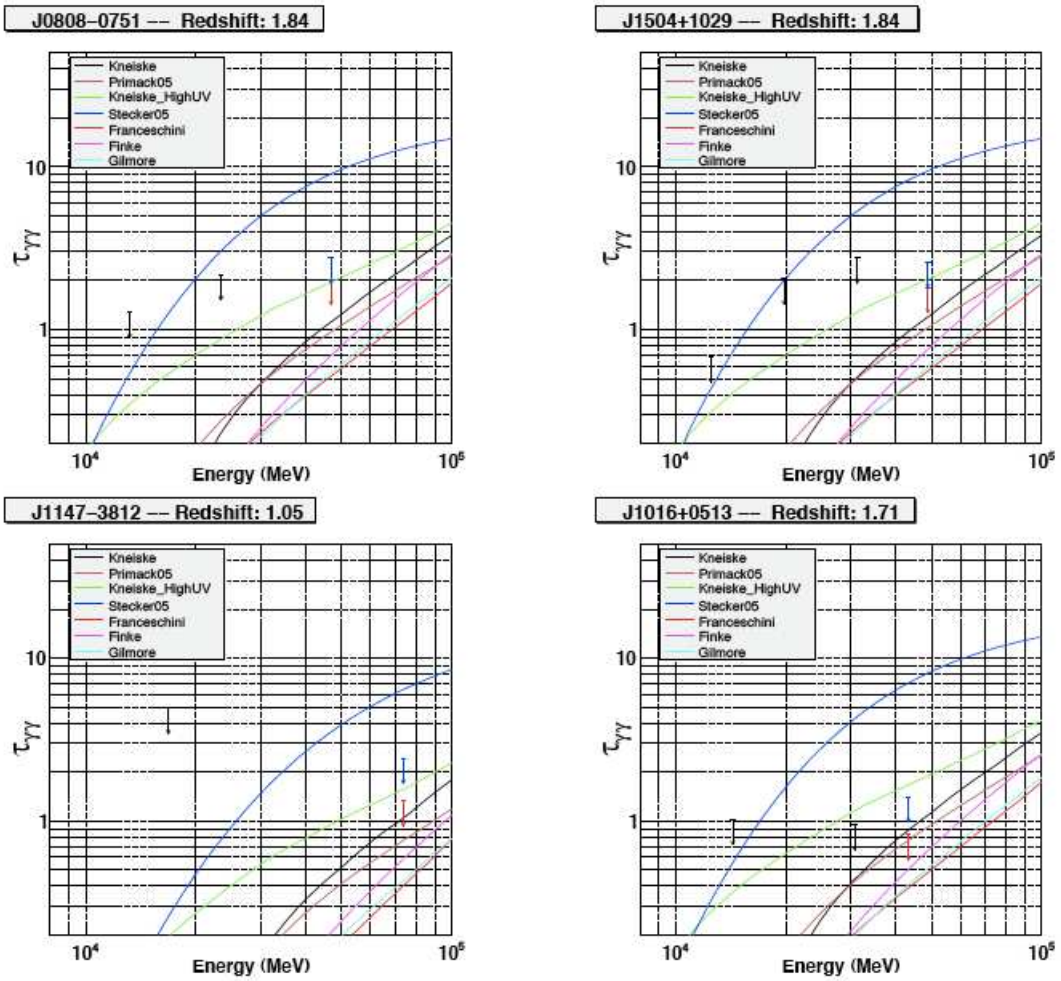

Figure 4.4: Derived upper limits for the optical depths of γ-rays emitted at z=1.84 (J0808-0751, J1505+1029), z=1.05 (J1147-3812) and z=1.71 (J1016+0513). Black arrows: upper limits at 95% confidence level in all energy bins used to determine the observed flux above 10 GeV. Red arrow: upper limits at 95% confidence level for the highest energy photon. Blue arrow: upper limit at 99% for the highest energy photon. The upper limits are inconsistent with the Stecker et al. (2006) EBL model. From Abdo et al. (2010d).

4.4 Our model

In this section we show our EBL model. The first step is computing the comoving emissivity or luminosity density (see section 4.4.1), then we integrate it over the redshift (see section 4.4.6) to obtain the specific intensity of the EBL. Results and comparison with other EBL model are shown in section 4.4.7.

4.4.1 Comoving emissivity

The comoving emissivity (or luminosity density) ϵ_ν at the cosmic time t per frequency unit (erg s^{-1} Hz^{-1} Mpc^{-3}) is:

$$\epsilon_\nu(t) = \int_{t_m}^{t} L_\nu(t - t')\dot{\rho}(t')dt' \tag{4.4.1}$$

where t_m is the cosmic time when the galaxy starts forming stars; L_ν is the galaxy luminosity, and $\rho(t)$ the star-formation rate.
Is more usefull to rewrite eq(4.4.1) in terms of redshift:

$$\epsilon_\nu(z) = \int_{z}^{\infty} L_\nu(t(z) - t(z'))\dot{\rho}(z') \left|\frac{dt}{dz'}\right| dz' \tag{4.4.2}$$

The emissivity depends upon the luminosity L_ν, star-formation rate ρ, cosmology dt/dz and on the evolution of the metallicity with the redshift. Each of these occupies a dedicated section.

4.4.2 Synthetic Galaxy Spectra

The claim of interpreting galaxy spectra in terms of their stellar spectra, led the astrophysical community to develop codes able to compute and predict the spectral evolution of a bunch of stars. The more recent models are based on the evolutionary population synthesis technique (e.g. Leitherer et al. 1999; 2010; Bruzual & Charlot 2003). Basically a set of input parameters, generally the stellar IMF, the star-formation rate of stars and the chemical

enrichment, are fixed. In this way a group of spectra of stars with different masses is generated and evolved along the Hertzprung-Russel diagram.
Our SEDs have been computed using the *STARBURST 99* code developed by Leitherer et al. (2010) and available online. The set of parameters fixed are the following. We select the classical Salpeter (1955) IMF, where the number of stars per unit of mass scales as $\xi(m) \sim m^{-2.35}$ with masses in the range $0.1 < m < 100$ $M_\odot$. In generating the SEDs, we adopted instantaneous star formation, i.e., stars are formed in a single burst, and their eventual evolution is described following the Padova evolutionary tracks. SEDs are computed for different fixed absolute metallicity Z (i.e. Z=0.04, Z=0.02, Z=0.008, Z=0.004, Z=0.001). In Fig. 4.8, the SEDs of coeval stellar population at different ages τ are shown. It is worth noting that because of the single star-formation burst, after 50 Myr the UV emission of stars drops quickly and the NIR component dominates stellar spectra.

4.4.3 Star-formation Rate History

The comoving emissivity in eq.(4.4.2) is the convolution of galaxy SEDs with $\dot{\rho}$ that represents the star-formation rate history, i.d. the number of solar masses produced per year in a comoving volume as a function of the redshift. A functional fit to observations of the star-formation rate history (SFH) up to redshift 4 has been proposed by Madau et al. (1996). In our work we use the observations collected by Hopkins & Beacom (2006) updated with the new measurements of Bouwens et al. (2007) and Reddy et al. (2008). The observational sample has been fitted by Li (2008) using the functional form proposed by Cole et al. (2001). The shape of the function is:

$$\dot{\rho}(z) = \frac{a + bz}{1 + (z/c)^d} \tag{4.4.3}$$

with (a,b,c,d) = (0.0157, 0.118, 3.23, 4.66). Data points and the fit (dotted line) are shown in Fig. 4.6 where it can be seen a rapid raise of the SFH up to redshift z=1, a flat shape in 1<z<4 range and a quick decline after redshift

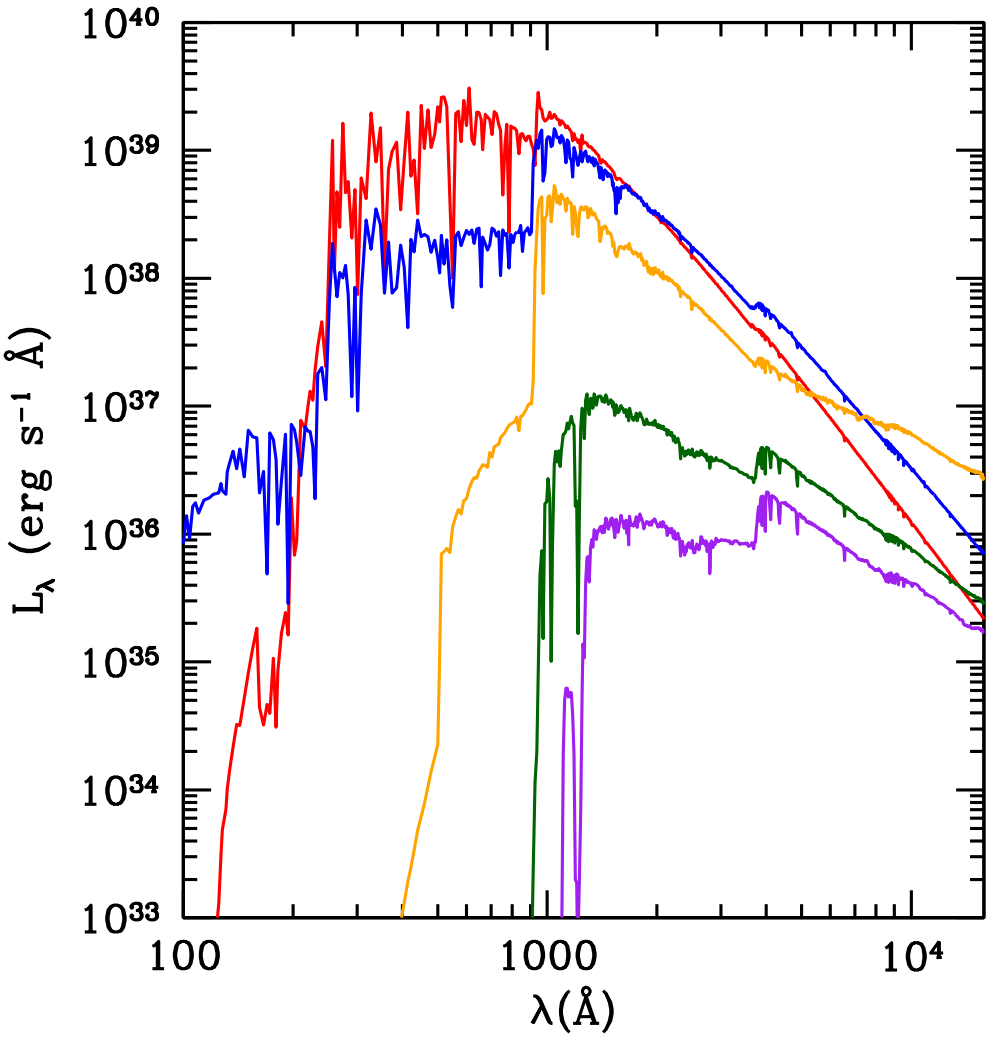

Figure 4.5: The synthetic galaxy spectra computed with STARBURST 99 with solar metallicity at different ages: instantaneous (red line), after 5 Myrs (blue line), after 50 Myrs (orange line) after 100 Myrs (green line) and after 200 Myrs (purple line)

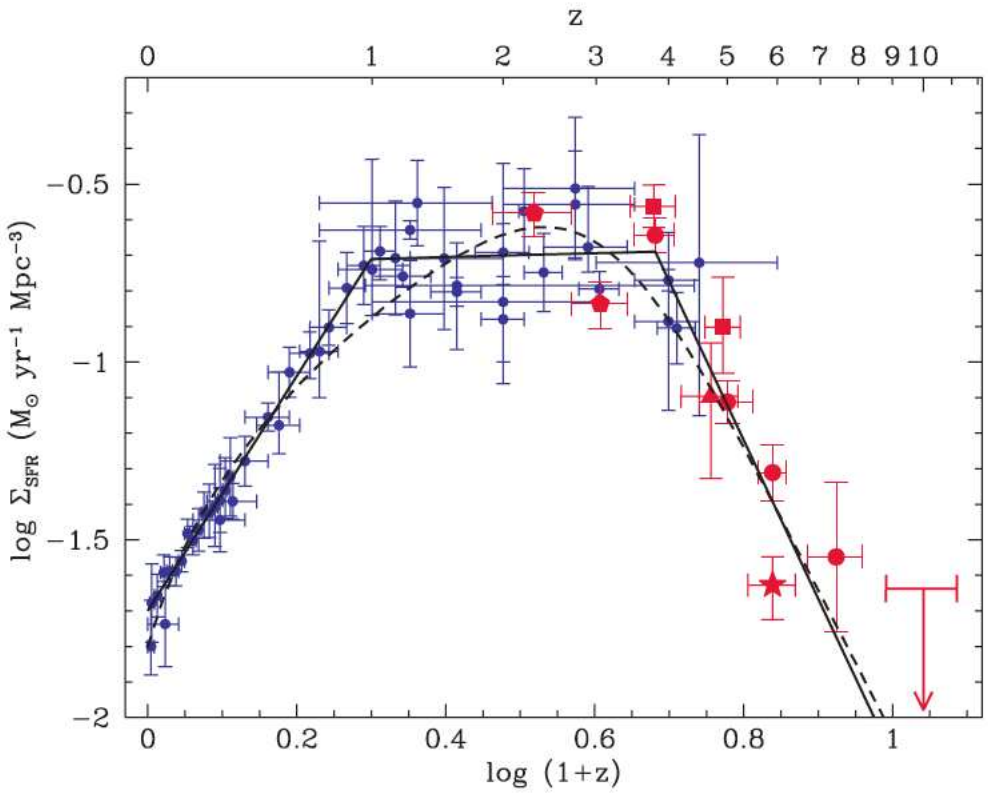

Figure 4.6: The updated cosmic star-formation history from Li (2008). The dotted line represent the updated fit to SFR we use.

4.

4.4.4 Redshift-Metallicity distribution

Observations indicate that metallicity in galaxies decreases with increasing the redshift. This phenomenological fact is in agreement with the hierarchical scenario of structure formation, in which metals are expelled in ISM by supernova explosions. Unfortunately different observational techniques give different evolution in redshift and numerical simulations are not fully reliable to give precise results.

In our work we refer to the observations of metallicity performed by Kewley & Kobulnicky (2005). They measure nebular oxygen abundances in star-

forming galaxies with magnitude M_B <-20.5 with redshift 0<z<3.5 finding that metallicity Z evolves as:

$$\frac{Z}{Z_\odot} \sim 10^{-\gamma z} \tag{4.4.4}$$

with $\gamma \sim 0.15$.

We implement in our calculation this redshift-metallicity law extrapolating it up to redshift z=9.

4.4.5 Dust absorption and re-emission

The UV and optical starlight is absorbed inside the galaxy by dust and re-emitted in IR band. To predict correctly the EBL we have to take into account such absorption and re-emission.

Different laws have been proposed to model the Milky Way (e.g. Cardelli, Claython & Mathis 1989) and the extragalactic absorption (e.g. Calzetti 2000; Kneiske et al. 2002) . Here we use a global extinction law as function of the cosmic metallicity. We assume that for super solar and solar metallicity, UV and optical photons are absorbed by the Cardelli law, proposed to model the Milky Way extinction. At lower metallicity we use the law proposed by Kneiske et al. (2002):

$$A_\lambda = 0.68 E(B-V) \cdot R \cdot (\lambda^{-1} - 0.35) \tag{4.4.5}$$

where $R = 0.32$. The free parameter of both extinction laws is the term $E(B-V)$ that has been fixed by fitting the observation of luminosity density at $\lambda = 1500$Å and $\lambda = 2800$Å (see Fig. 4.9 and Fig. 4.10). We found $E(B-V) = 0.16$ for Cardelli law and $E(B-V) = 0.25$ for Kneiske model. The absorption coefficient is:

$$g(\lambda) = 10^{-0.4 A_\lambda} \tag{4.4.6}$$

Applying this coefficient to synthetic intrinsic spectra L_λ^{int} we have

$$L_\lambda^{abs} = L_\lambda^{int} \cdot g(\lambda) \tag{4.4.7}$$

The intergalactic medium is composed by three different components (see Desert et al. 1990):

- *big grains*: large grains (15-110 nm) absorb mainly optical starlight and re-emit in the FIR band;
- *very small grains*: UV starlight is mainly absorbed by small grains (1.2-15 nm) that re-emit in NIR band;
- *PAH component* a third component is due to the so-called polycyclic aromatic hydrocarbons (PAHs) (0.4-1.2 nm) that re-emit as a broad emission lines at 10 μm.

We assume that dust is in thermodynamic equilibrium and thus that its re-emission spectrum is the sum of three blackbodies at three different temperatures:

$$L_\lambda^{dust} = \sum_{i=1}^{3} c_i \cdot B_\lambda(\mathrm{T_i}) \tag{4.4.8}$$

where B_λ is the Planck function and where the coefficients c_i have been obtained as follows: Spinoglio et al.(1995) proposed a linear relation between bolometric luminosity and IR luminosity in four IR bands, using non-Seyfert galaxies. We fitted this four points with a function sum of three blackbodies obtaining c_i and T_i with the trial and error method. The temperature that we obtain from the fit are T=35 K for the cold component, T=70 K for the warm component and T=240 K for the PAH component. This values are in agreement with Kneiske et al. (2002) and by Finke, Razzaque & Dermer (2010). The resulting total spectra are thus:

$$L_\lambda^{tot} = L_\lambda^{int} \cdot g(\lambda) + A \cdot L_\lambda^{dust} \tag{4.4.9}$$

where A represents the normalization due to energy conservation of the absorbed and re-emitted photons.

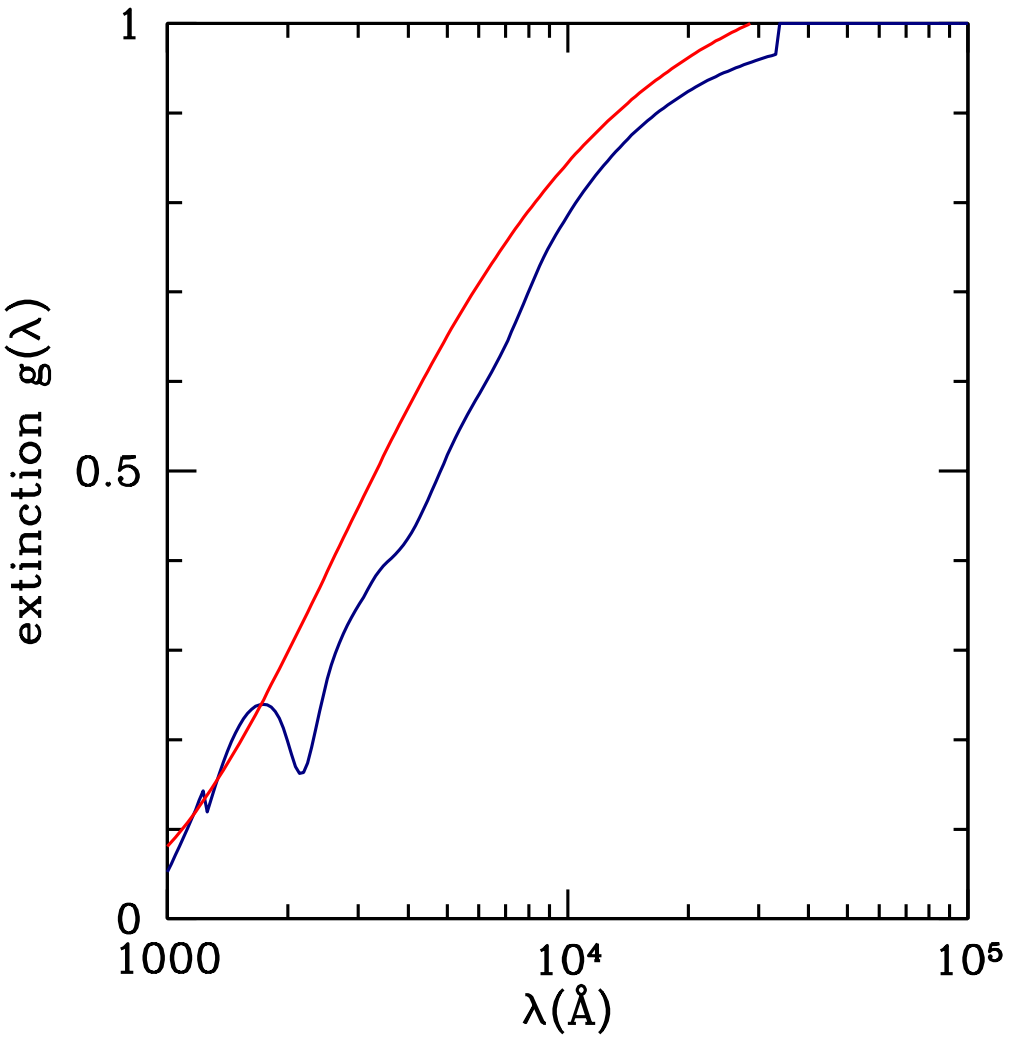

Figure 4.7: The extinction law used by Kneiske et al. (2002) (red line) and the Cardelli, Clayton & Mathis galactic extinction law (1989) (blue line).

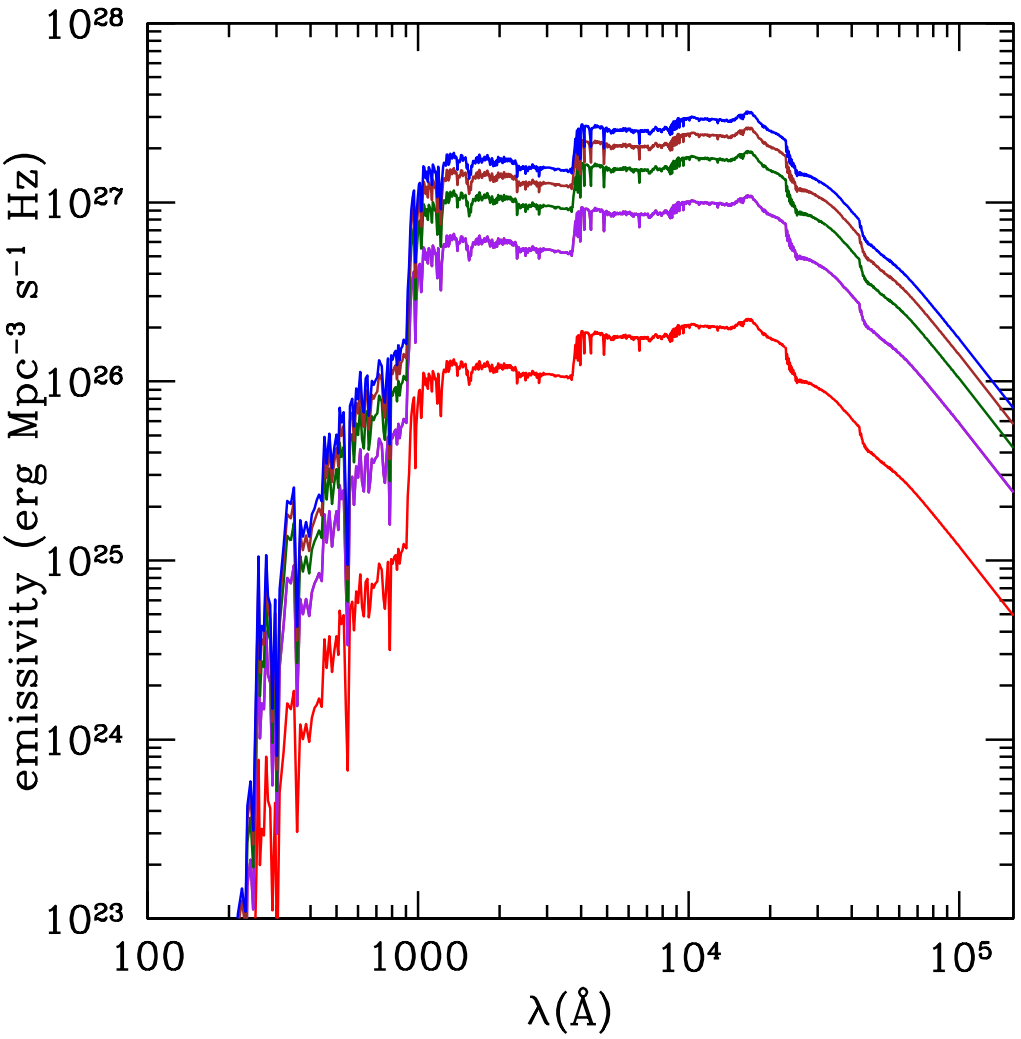

Figure 4.8: Intrinsic (no absorption and no dust re-emission) emissivities at different redshift: z=0 (red line), z=0.5 (purple line), z=1.0 (dark green line), z=1.5 (brown line) and z=2.0 (blue line).

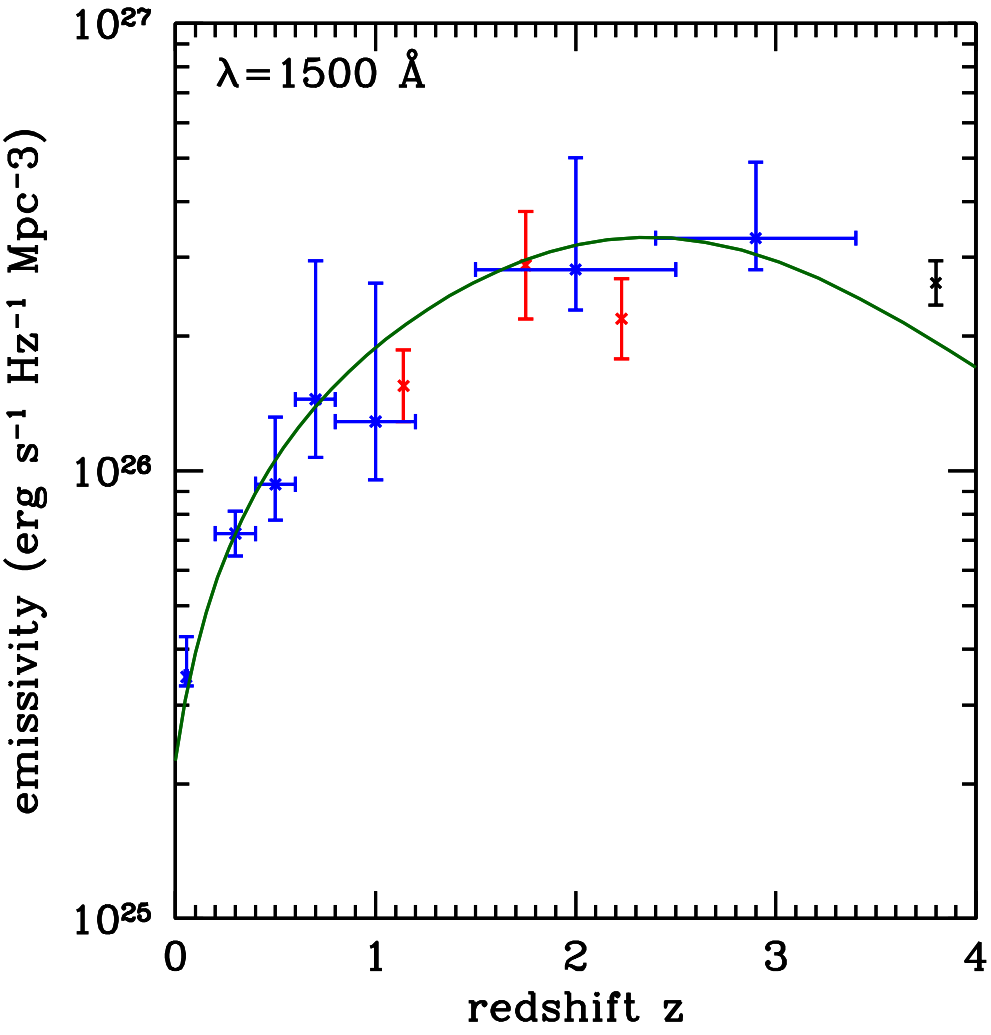

Figure 4.9: Our comoving emissivity (dark green line) at 1500 Å and the observations of Schiminovich et al. (2005) in red, Dahlen et al. (2007) in blue and Bouwens et al. (2007) in black.

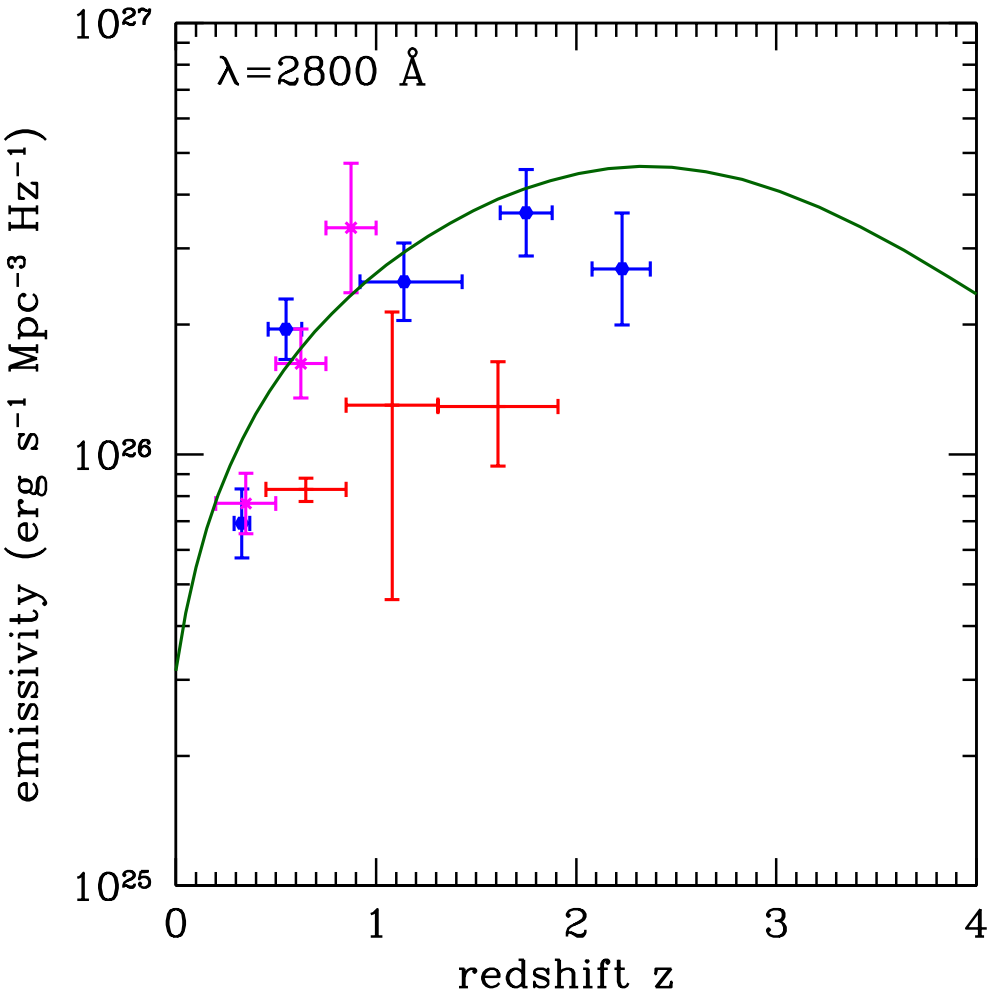

Figure 4.10: Our comoving emissivity (dark green line) at 2800 Å and the observations of Gabash et al. in red, Dahlen et al. (2006) in blue and Lilly et al. (1996) in magenta.

4.4.6 Extragalactic background light model

The synthetic spectra obtained adding the absorption and re-emission by dust have been convolved with the SFH has shown in the previous section. Here the specific intensity of the radiation field is given by:

$$J_\nu(z_0) = \frac{(1+z_0)^3}{4\pi} \int_{z_0}^{\infty} \epsilon_{\nu'}(z) e^{-\tau} \frac{dl}{dz} dz, \tag{4.4.10}$$

where $\nu' = \nu(1+z)/(1+z_0)$, and τ is the effective optical depth due to absorption in the clumpy IGM:

$$\tau_{eff}(\nu_0, z_0, z) = \int_{z_0}^{z} dz' \int_0^{\infty} dN_{HI} \frac{\partial^2 N}{\partial N_{HI} \partial z'} (1 - e^{-\tau}) \tag{4.4.11}$$

where τ is the Lyman-continuum (LyC) optical depth through a given cloud, and the term $\partial^2/(\partial N_{HI} \partial z')$ is the absorber distribution given by:

$$\frac{\partial^2 N}{\partial N_{HI} \partial z} \propto N_{HI}^{-1.5} (1+z)^\gamma \tag{4.4.12}$$

with $\gamma = 1.5$. The fraction of ionizing radiation escaping from galaxies has been set to 0.1. Moreover we neglect quasar emission. We performed this computation with the code CUBA (Haardt & Madau 1996), a radiative transfer code that follows the propagation of LyC photons through a partially ionized inhomogeneous IGM. CUBA outputs have been extensively used to model the Lyα forest in large cosmological simulations (e.g. Tytler et al. 2004; Theuns et al. 1998; Davé et al. 1997; Zhang et al. 1997). In Madau, Haardt, & Rees (1999) the focus was on the candidate sources of photoionization at early times and on the history of the transition from a neutral IGM to one that is almost fully ionized. The inclusion of updated ionizing and IR emissivity due to galaxies is in the new version of the code (Haardt & Madau 2011).

Our model is shown in Fig.4.11 where the redshift evolution is displayed while a comparison with the other more recent models is shown in Fig.4.3.

4.4.7 Comparison with other models

Our EBL model belongs to the so-called semi-empirical models where the synthetic galaxy spectra are convolved with the observed cosmic starformation history. The models of Kneiske & Dole (2010) and Finke, Razzaque & Dermer (2010) belong to this class. The overall treatment is similar although we use different IMF, cosmic star-formation fit and absorption law. Moreover we include the metallicity-redshift relation and the extinction of the ionizing radiation by IGM.

As shown by Fig. 4.3 the main difference of our EBL with other models lies in the optical and MIR region. Because of the chose of IMF of stars in galaxies combined with the extinction law we obtain a very low optical contribution, lower then other models but in agreement with galaxy counts (Madau & Pozzetti 2000; Fazio et al. 2004).

In the MIR region the re-emission of dust starts dominating. We predict the lower value at 10 μm due to our dust model. In particular changing the coefficient c_i, that give the weight of a precise dust component a different shape in MIR band can be obtained. At higher wavelength, up to 100 μm, we are in good agreement with the model of Franceschini, Rodighiero & Vaccari (2008).

4.4.8 γ-ray optical depth

It is well known that when a photon with energy E_1 interact with a second photon with energy E_2 with an angle of incidence θ in the centre of mass of the system and the following condition is verified:

$$\sqrt{2E_1E_2(1-\cos\theta)} \geq 2m_ec^2 \tag{4.4.13}$$

an electron/proton pair is generated. Thus the minimum energy the target photon to pair-produce is:

$$E_{th} = \frac{2m_e^2c^4}{E_\gamma(1-\cos\theta)} \tag{4.4.14}$$

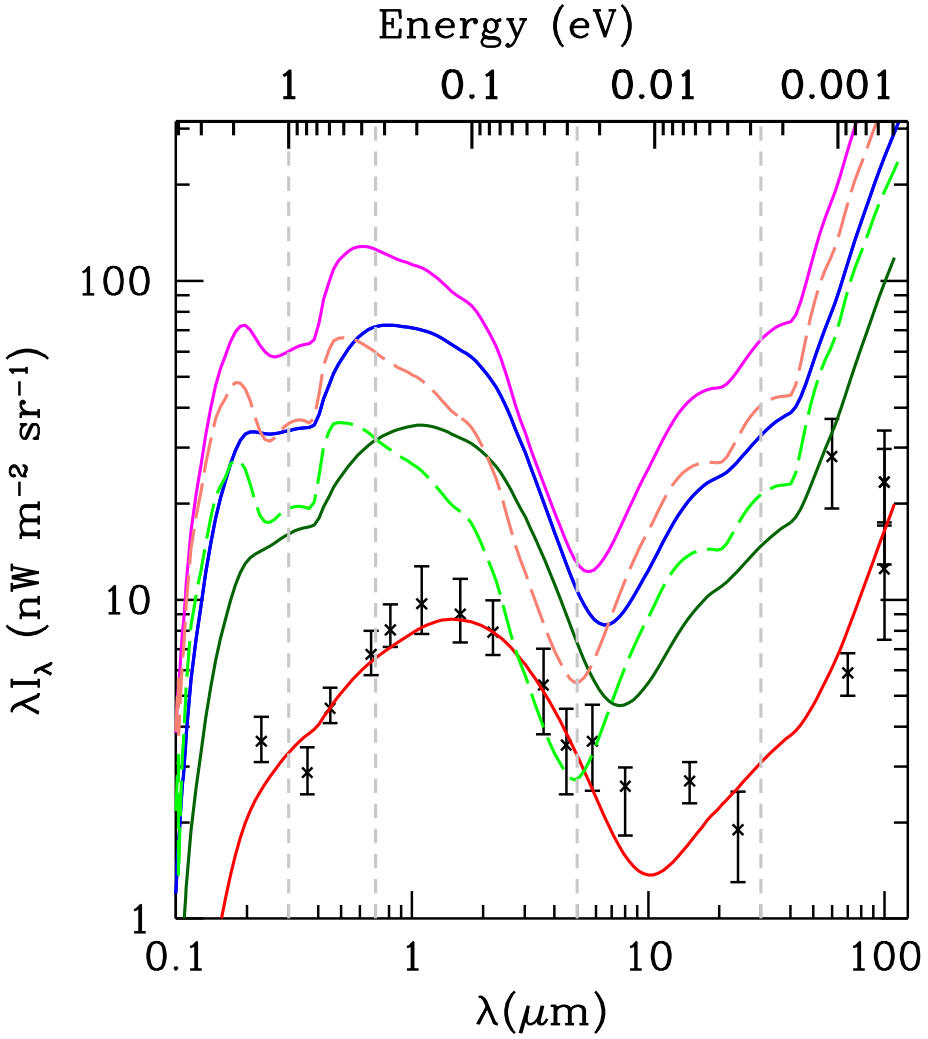

Figure 4.11: The EBL at different redshifts: z=0 (red line), z=0.5 (dark green line), z=1 (blue line), z=2 (magenta line), z=4 (salmon dotted line) and z=5 (green dotted line).

where E_γ is the incident photon energy.

The cross section for this process (Gould & Schreder 1967) is:

$$\sigma(E_1, E_2, \theta) = \frac{3\sigma_T}{16}(1-\beta^2)\left[2\beta(\beta^2-2) + (3-\beta^4)ln\left(\frac{1+\beta}{1-\beta}\right)\right] \quad (4.4.15)$$

where

$$\beta = \sqrt{1 - \frac{2m_e c^4}{E_1 E_2(1-\cos\theta)}} \quad (4.4.16)$$

and σ_T is the Thomson cross section.

The optical depth of attenuation of a photon with energy E_γ traveling in a photon field with number density $n(E_{bkg}, z)$ is:

$$\tau(E_\gamma, z_0) = \frac{1}{2}\int_0^{z_0} dz \frac{dl}{dz}\int_{-1}^{1} d(\cos\theta)(1-\cos\theta) \times \int_{E_m in}^{\infty} dE_{bkg} n(E_{bkg}, z)\sigma(E_\gamma(1+z), E_{bkg}, \theta) \quad (4.4.17)$$

where

$$E_{min} = \frac{E_{th}}{1+z} = \frac{2m_e^2 c^4}{E_\gamma(1-\cos\theta)(1+z)} \quad (4.4.18)$$

and dl/dz is the cosmological line element.

We have computed the optical depth of γ-ray at different redshift and energies for our model. The results are shown in Fig.4.12. The increase of star-formation rate between present day and z=1 leads the optical depth to grow rapidly as can be infer from Fig.4.12.

4.5 Conclusions

We have proposed a new theoretical model for the UV through FIR EBL from direct stellar radiation and radiation emitted by dust. The model belongs to the so-called *semi-empirical model* group in which synthetic galaxy spectra are convolved with the SFH and dust re-emission is computed theoretically.

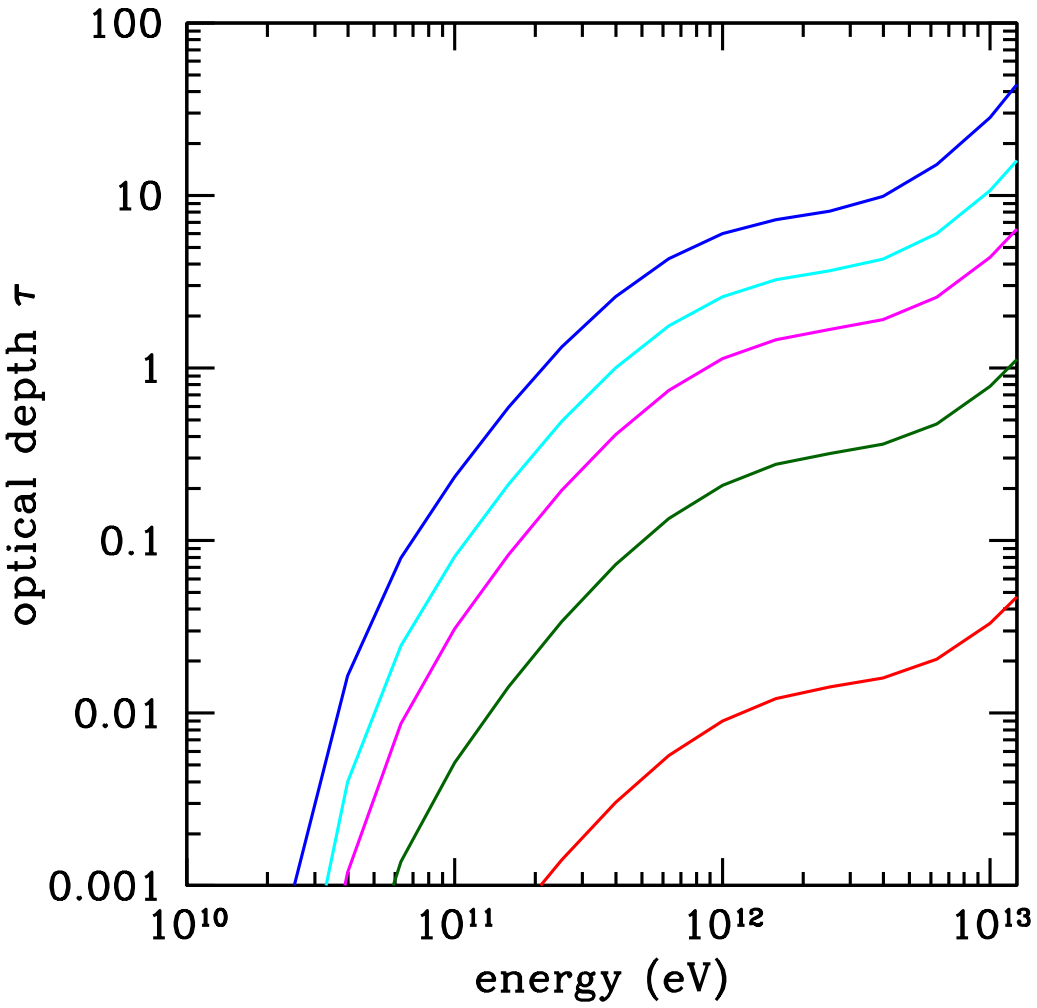

Figure 4.12: Optical depth at different low redshifts: z=0.001 (red line), z=0.02 (dark green line), z=0.1 (magenta line) z=0.2 (cyan line) and z=0.5 (blue line).

Differently to the other models belonging to this class (Kneiske & Dole 2010; Finke Razzaque & Dermer 2010), we have taken into account two extinction laws as a function of the cosmic metallicity and metallicity-redshift relation (Kewley & Kobulnicky 2005). Furthermore we have employed the code CUBA (Haardt & Madau 1996; 2011) to integrate the comoving emissivity over the redshift, taking into account the absorption of ionizing radiation due to the IGM.

Our model is consistent with the most reliable SFH data (Li 2008) and results to be in good agreement with the luminosity density observations at different wavelengths. Furthermore the energy density of our EBL model is consistent with the EBL data at redshift z=0 and it results compatible with lower limits from galaxy counts (Madau & Pozzetti 2000; Fazio et al. 2004) in the optical and NIR band.

The optical depth of γ-rays has been computed for different value of redshift and energy. We found that the Universe is transparent in the γ-ray band ($\tau << 1$) for energy lower the 20 GeV at any redshift in fully agreement with the other EBL models (Kneiske & Dole 2010; Franceschini Rodighiero & Vaccani 2008; Gilmore et al. 2009; Finke Razzaque & Dermer 2010). Further constraints on $\gamma\gamma$ opacity and thus on the EBL could come from blazar observations with the next generation of Cherenkov telescopes, CTA.

Chapter 5

Summary and conclusions

In this Thesis I have dealt with three “hot topics" in the extragalactic very high energy (VHE) astrophysics in which blazars have a significant role: the extragalactic background light (EBL), the intergalactic magnetic field (IGMF), and the extragalactic γ-ray background (EGB).

First, I have computed the contribution of blazars (FSRQs and BL-Lacs) to the total *Fermi*-LAT EGB with two basic assumptions. First, I assumed that radio galaxies (FRI and FRII) are the parental populations of blazars (BL-Lacs and FSRQ respectively), and thus that the radio luminosity function (LF) of radio galaxies can be used as a proxy for the blazar LF in the γ-ray band. Second, that the blazar spectral energy distribution (SED) can be described by the blazar sequence proposed by Fossati et al. (1998). From these starting points, I fitted the blazar *Fermi*-LAT logN-LogS. The fit gives the ratio of blazars per radio galaxy, and predict the relative number of FSRQs and BL-Lacs, consistent with the beaming model of blazars.

Then I computed the contribution of resolved and unresolved blazars to the EGB. I found that our model can account for the 45% of the *Fermi*-LAT EGB, and it is in good agreement with intermediate (1-30 GeV) energy data. Blazars are not able to explain the low energy EGB component (0.1-10 GeV) and the very high energy band (50-100 GeV) where $\gamma\gamma$ absorption dominates.

I showed how γ-ray emission from star-forming galaxies seen as sources of

cosmic rays and subsequent pion decay (Stecker & Venters 2010) can explain the low energy data, while high energy data can be explained in terms of local DM annihilation. Following the recipes of Ando (2005), I modeled γ-ray emission of galactic DM relics with two free parameters: the annihilation cross section and mass of DM particles. By fitting *Fermi*-LAT data with blazars, galaxies, and DM emission, I could put upper limits for the cross section and mass of DM particles.

Blazars can also be used to put a lower limit on the intensity of the IGMF. The basic idea is to study the reprocessed emission in TeV detected blazars. The ideal candidates for this study are blazars detected in the TeV band at redshifts z>0.1, that do not show any emission in the *Fermi*-LAT band. The secondary emission is due to CMB photons upscattered by electron/positron pairs generated by primary TeV photons absorbed by the EBL. The possible presence of an IGMF deflects pairs away from the line of sight, resulting in a suppression of the secondary emission. Therefore the detection or upper limits in the GeV band obtained with *Fermi*-LAT can in principle constrain the intensity of any IGMF. In this framework I computed the cascade emission from the TeV source 1ES 0229+200 with a semi-analytic model by taking into account the effect of the time delay between primary and secondary emission, which plays a very significant role in assessing the value of the IGMF. Assuming that 1ES 0229+200 has been constantly active during the period of 3-4 years of TeV observations, we could obtain a lower limit for the IGMF of $B_{IGMF} \geq 10^{-18}$G. This value results to be lower than similar previous estimates obtained without taking into account the effect of time delay (Neronov & Vovk; Tavecchio et al. 2010; 2011). Finally I have presented a new theoretical model for the EBL, from UV to FIR band. The model is based on a semi-empirical approach. I convolved the synthetic galaxy spectra, obtained with STARBURST99 (Leitherer et al. 1999) with the redshift dependent star formation rate (see e.g., Li 2008), adopting the redshift-metallicity law proposed by Kewley & Kobulnicky (2005). As optical-UV radiation is ab-

sorbed and re-emitted by dust in the interstellar medium, I used a metallicity dependent extinction law for absorption, and then modeled the re-emission by dust as the sum of three black-bodies at different temperatures (Kneiske et al. 2002). The resulting comoving emissivity has been integrated over the redshift with the code CUBA (Haardt & Madau 1996; 2011). Our model results to be in agreement with EBL observations at redshift z=0 and with the luminosity density data at 1500Å and 2800Å. The main uncertainties concern on the modeling of dust absorption of optical-UV radiation, and re-emission in the IR band.

In the next years a substantial improvement on our knowledge of the EBL, IGMF and EGB is expected. In particular, the next generation of Cherenkov ground-based telescopes (CTA) should be able to perform simultaneous observations in the GeV and TeV bands. This will producing more accurate lower limits on the IGMF also will permit improved studies of the γ-ray opacity of the Universe. New observations of EGB at energies up to 300 GeV are expected from *Fermi*-LAT. These new data could give new information on the role played by DM annihilation in our Galaxy. Furthermore, determination of the γ-ray LF of FSRQs and BL-Lacs will constrain the blazar component of the EGB.

The Thesis work produced so far the following papers:

- *Cavadini M.*, Salvaterra R., Haardt F., 2011, arXiv, arXiv:1105.4613
- Dermer C. D., *Cavadini M.*, Razzaque S., Finke J. D., Chiang J., Lott B., 2011, ApJ, 733, L21

A third paper focused on EBL and $\gamma\gamma$ opacity is in preparation.

Bibliography

Abazajian K. N., Blanchet S., Harding J. P., 2010a, arXiv:1012.1247

Abazajian K. N., Blanchet S., Harding J. P., 2010b, arXiv:1011.5090

Abdo A. A., et al., 2009, ApJ, 700, 597

Abdo A. A., et al., 2010a, PhRvL, 104, 101101

Abdo A. A., et al., 2010b, ApJ , 720, 435

Abdo A. A., et al., 2010c, ApJ, 723, 1082

Abdo A. A., et al., 2010d, ApJ, 720, 912

Abdo A. A., et al., 2010e, ApJ, 715, 429

Aharonian F. A., Coppi P. S., Voelk H. J., 1994, ApJ, 423, L5

Aharonian, F. A., Volk, H. J. 2001, American Institute of Physics Conference Series, 558

Aharonian F., "Very high energy cosmic gamma radiation : a crucial window on the extreme Universe", River Edge, NJ: World Scientific Publishing (512pp), 2004

Aharonian F., et al., 2006, Natur, 440, 1018

Aharonian F., et al., 2007, A&A, 475, L9

Ando S., 2005, PhRvL, 94, 171303

Atwood W. B., et al., 2009, ApJ, 697, 1071

Barrow J. D., Ferreira P. G., Silk J., 1997, PhRvL, 78, 3610

Bauermeister A., Blitz L., Ma C.-P., 2010, ApJ, 717, 323

Berezinsky V. S., Blasi P., Ptuskin V. S., 1997, ApJ, 487, 529

Berezinsky V., Gazizov A., Kachelrieß M., Ostapchenko S., 2011, PhLB, 695, 13

Béthermin M., Dole H., Beelen A., Aussel H., 2010, A&A, 512, A78

Biermann L., 1950, ZNatA, 5, 65

Blasi P., Burles S., Olinto A. V., 1999, ApJ, 514, L79

Bigiel F., Leroy A., Walter F., Brinks E., de Blok W. J. G., Madore B., Thornley M. D., 2008, AJ, 136, 2846

Bignami G. F., Hermsen W., 1983, ARA&A, 21, 67

Błażejowski M., Sikora M., Moderski R., Madejski G. M., 2000, ApJ, 545, 107

Bonometto S., Rees M. J., 1971, MNRAS, 152, 21

Böttcher M., Dermer C. D., Finke J. D., 2008, ApJ, 679, L9

Borione A., et al., 1994, NIMPA, 346, 329

Bouwens R. J., Illingworth G. D., Franx M., Ford H., 2007, ApJ, 670, 928

Bruzual A. G., Charlot S., 1993, ApJ, 405, 538

Bruzual G., Charlot S., 2003, MNRAS, 344, 1000

Calzetti D., Armus L., Bohlin R. C., Kinney A. L., Koornneef J., Storchi-Bergmann T., 2000, ApJ, 533, 682

Cambrésy L., Reach W. T., Beichman C. A., Jarrett T. H., 2001, ApJ, 555, 563

Cardelli J. A., Clayton G. C., Mathis J. S., 1989, ApJ, 345, 245

Chaves R. C. G., for the H. E. S. S. Collaboration, 2009, arXiv, arXiv:0907.0768

Chary R.-R., Pope A., 2010, arXiv, arXiv:1003.1731

Chiang J., Fichtel C. E., von Montigny C., Nolan P. L., Petrosian V., 1995, ApJ, 452, 156

Cirasuolo M., McLure R. J., Dunlop J. S., Almaini O., Foucaud S., Simpson C., 2010, MNRAS, 401, 1166

Cole S., et al., 2001, MNRAS, 326, 255

Colin P., et al., 2009, arXiv, arXiv:0907.0960

Coppi P. S., Aharonian F. A., 1997, ApJ, 487, L9

Dahlen T., Mobasher B., Dickinson M., Ferguson H. C., Giavalisco M., Kretchmer C., Ravindranath S., 2007, ApJ, 654, 172

Davé R., Hellsten U., Hernquist L., Katz N., Weinberg D. H., 1998, ApJ, 509, 661

D'Avezac P., Dubus G., Giebels B., 2007, A&A, 469, 857

Dermer C. D., 1986, A&A, 157, 223

Dermer C. D., Schlickeiser R., 1993, ApJ, 416, 458

Dermer C. D., 2007, ApJ, 659, 958

Dermer C. D., Menon G., 2009, herb.book,

Desert F.-X., Boulanger F., Puget J. L., 1990, A&A, 237, 215

Dolag K., Kachelrieß M., Ostapchenko S., Tomàs R., 2009, ApJ, 703, 1078

Dolag K., Kachelriess M., Ostapchenko S., Tomàs R., 2011, ApJ, 727, L4

Domínguez A., et al., 2011, MNRAS, 410, 2556

Donato D., Ghisellini G., Tagliaferri G., Fossati G., 2001, A&A, 375, 739

Draper A. R., Ballantyne D. R., 2009, ApJ, 707, 778

Dunlop J. S., Peacock J. A., 1990, MNRAS, 247, 19

Elyiv A., Neronov A., Semikoz D. V., 2009, PhRvD, 80, 023010

Enomoto, R., Mori, M., & Tanagita, S. 2003, The Universe Viewed in Gamma-Rays; International Science Symposium held September 25-28, 2002, in Kashiwa, Chiba, Japan. Edited by R. Enomoto, M. Mori, and S. Tanagita. Frontiers Science Series No. 39. AB471.A1 I565 2002; ISSN 0915-8502; ISBN 4-946443-75-4. Published by the universal Academy Press, Inc., Tokyo, Japan, 2003.,

Essey W., Kalashev O. E., Kusenko A., Beacom J. F., 2010, PhRvL, 104, 141102

Fanaroff B. L., Riley J. M., 1974, MNRAS, 167, 31P

Faucher-Giguère C.-A., Loeb A., 2010, JCAP, 1, 5

Fazio G. G., Stecker F. W., 1970, Nature, 226, 135

Fazio G. G., et al., 2004, ApJS, 154, 39

Ferrarese L., Ford H., 2005, SSRv, 116, 523

The Fermi-LAT collaboration, 2011, arXiv, arXiv:1108.1420

Fichtel C. E., Simpson G. A., Thompson D. J., 1978, ApJ, 222, 833

Fields B. D., Pavlidou V., Prodanović T., 2010, ApJ, 722, L199

Finkbeiner D. P., Davis M., Schlegel D. J., 2000, ApJ, 544, 81

Finke J. D., Razzaque S., Dermer C. D., 2010, ApJ, 712, 238

Fossati G., Maraschi L., Celotti A., Comastri A., Ghisellini G., 1998, MNRAS, 299, 433

Franceschini A., Rodighiero G., Vaccari M., 2008, A&A, 487, 837

Frayer D. T., et al., 2006, ApJ, 647, L9

Gabasch A., et al., 2004, A&A, 421, 41

Georganopoulos M., Finke J. D., Reyes L. C., 2010, ApJ, 714, L157

Ghirlanda G., Ghisellini G., Tavecchio F., Foschini L., Bonnoli G., 2011, MNRAS, 413, 852

Ghisellini G., Celotti A., Fossati G., Maraschi L., Comastri A., 1998, MNRAS, 301, 451

Ghisellini G., Celotti A., 2001, A&A, 379, L1

Ghisellini G., Tavecchio F., 2008, MNRAS, 387, 1669

Ghisellini G., et al., 2010, MNRAS, 405, 387

Gilli R., Comastri A., Hasinger G., 2007, A&A, 463, 79

Gilmore R. C., Madau P., Primack J. R., Somerville R. S., Haardt F., 2009, MNRAS, 399, 1694

Gilmore R. C., Somerville R. S., Primack J. R., Domínguez A., 2011, arXiv, arXiv:1104.0671

Gnedin N. Y., Ferrara A., Zweibel E. G., 2000, ApJ, 539, 505

Gnedin N. Y., Tassis K., Kravtsov A. V., 2009, ApJ, 697, 55

Gould R. J., Schréder G. P., 1967, PhRv, 155, 1408

Grasso D., Rubinstein H. R., 2001, PhR, 348, 163

Haardt F., Madau P., 1996, ApJ, 461, 20

Haardt F., Madau P., 2011, arXiv, arXiv:1105.2039

Hartman R. C., et al., 1999, ApJS, 123, 79

Hauser M. G., Dwek E., 2001, ARA&A, 39, 249

Holder J., 2007, sngh.conf, 69

Hopkins A. M., Beacom J. F., 2006, ApJ, 651, 142

Inoue, Y., & Totani, T. 2009, ApJ, 702, 523

Jedamzik K., Katalinić V., Olinto A. V., 2000, PhRvL, 85, 700

Jungman G., Kamionkowski M., Griest K., 1996, PhR, 267, 195

Juvela M., Mattila K., Lemke D., Klaas U., Leinert C., Kiss C., 2009, A&A, 500, 763

Kewley L., Kobulnicky H. A., 2005, ASSL, 329, 307

Kneiske T. M., Dole H., 2008, AIPC, 1085, 620

Inoue Y., Totani T., 2009, ApJ, 702, 523

Kneiske T. M., Mannheim K., 2008, A&A, 479, 41

Kneiske T. M., Dole H., 2008, AIPC, 1085, 620

Kulsrud R., Cowley S. C., Gruzinov A. V., Sudan R. N., 1997, PhR, 283, 213

Kushida J., Tanimori T., Kubo H., CANGAROO team, 2003, ICRC, 4, 2493

Lagache G., Haffner L. M., Reynolds R. J., Tufte S. L., 2000, A&A, 354, 247

Leitherer C., et al., 1999, ApJS, 123, 3

Leroy A. K., Walter F., Brinks E., Bigiel F., de Blok W. J. G., Madore B., Thornley M. D., 2008, AJ, 136, 2782

Levenson L. R., Wright E. L., 2008, ApJ, 683, 585

Li L.-X., 2008, MNRAS, 388, 1487

Lilly S., et al., 1998, ApJ, 500, 75

Madau P., Ghisellini G., Fabian A. C., 1994, MNRAS, 270, L17

Madau P., Ferguson H. C., Dickinson M. E., Giavalisco M., Steidel C. C., Fruchter A., 1996, MNRAS, 283, 1388

Madau P., Pozzetti L., 2000, MNRAS, 312, L9

Madau P., Haardt F., Rees M. J., 1999, ApJ, 514, 648

Madsen M. S., 1989, MNRAS, 237, 109

Mannheim K., 1993, A&A, 269, 67

Maraschi L., Ghisellini G., Celotti A., 1992, ApJ, 397, L5

Matsumoto T., et al., 2005, ApJ, 626, 31
Mazin D., PhD Thesis, 2007

Mazin D., Raue M., 2007, A&A, 471, 439

McLure R. J., Kukula M. J., Dunlop J. S., Baum S. A., O'Dea C. P., Hughes D. H., 1999, MNRAS, 308, 377

Metcalfe L., et al., 2003, A&A, 407, 791

Mori M., 1997, ApJ, 478, 225

Mücke A., Pohl M., 2000, MNRAS, 312, 177

Murase K., Takahashi K., Inoue S., Ichiki K., Nagataki S., 2008, ApJ, 686, L67

Narumoto T., Totani T., 2006, ApJ, 643, 81

Neronov A., Semikoz D. V., 2009, PhRvD, 80, 123012

Neronov A., Vovk I., 2010, Sci, 328, 73

Neronov A., Semikoz D. V., 2011, arXiv, arXiv:1103.3484

Olive K. A., Steigman G., Walker T. P., 2000, PhR, 333, 389

Orr M. R., Krennrich F., Dwek E., 2011, ApJ, 733, 77

Padovani P., Ghisellini G., Fabian A. C., Celotti A., 1993, MNRAS, 260, L21
Peacock J. A., Cosmological physics, Cambridge U Press

Perkins J. S., VERITAS Collaboration, 2010, HEAD, 42, 708

Plaga R., 1995, Natur, 374, 430

Primack J. R., Bullock J. S., Somerville R. S., 2005, AIPC, 745, 23

Pudritz R. E., Silk J., 1989, ApJ, 342, 650

Reddy N. A., Steidel C. C., Pettini M., Adelberger K. L., Shapley A. E., Erb D. K., Dickinson M., 2008, ApJS, 175, 48

Rees M. J., 1984, ARA&A, 22, 471

Salpeter E. E., 1955, ApJ, 121, 161

Schiminovich D., et al., 2005, ApJ, 619, L47

Schramm D. N., Turner M. S., 1998, RvMP, 70, 303

Setti G., Woltjer L., 1989, A&A, 224, L21

Somerville R. S., Primack J. R., 1999, MNRAS, 310, 1087

Somerville R. S., Primack J. R., Faber S. M., 2001, MNRAS, 320, 504

Spinoglio L., Malkan M. A., Rush B., Carrasco L., Recillas-Cruz E., 1995, ApJ, 453, 616

Sreekumar P., et al., 1998, ApJ, 494, 523

Stecker F. W., de Jager O. C., Salamon M. H., 1992, ApJ, 390, L49

Stecker F. W., Salamon M. H., Malkan M. A., 1993, ApJ, 410, L71

Stecker F. W., Salamon M. H., 1996, ApJ, 464, 600

Stecker F. W., Malkan M. A., Scully S. T., 2006, ApJ, 648, 774

Stecker F. W., Venters T. M., 2010, arXiv, arXiv:1012.3678

Strong A. W., Moskalenko I. V., Reimer O., 2004, ApJ, 613, 956

Tavecchio F., Ghisellini G., Foschini L., Bonnoli G., Ghirlanda G., Coppi P., 2010, MNRAS, 406, L70

Tavecchio F., Ghisellini G., Bonnoli G., Foschini L., 2011, MNRAS, 414, 3566

Taylor A. M., Vovk I., Neronov A., 2011, A&A, 529, A144

Taylor G. B., Barton E. J., Ge J., 1994, AJ, 107, 1942

Theuns T., Leonard A., Efstathiou G., Pearce F. R., Thomas P. A., 1998, MNRAS, 301, 478

Tytler D., et al., 2004, ApJ, 617, 1

Ullio P., Bergström L., Edsjö J., Lacey C., 2002, PhRvD, 66, 123502

Urry C. M., Padovani P., 1995, PASP, 107, 803

Venters T. M., Pavlidou V., 2011, ApJ, 737, 80

Widrow L. M., 2002, RvMP, 74, 775

Willott C. J., Rawlings S., Blundell K. M., Lacy M., Eales S. A., 2001, MNRAS, 322, 536

Wright E. L., 2004, NewAR, 48, 465

Zhang Y., Anninos P., Norman M. L., Meiksin A., 1997, ApJ, 485, 496

Zeldovich I. B., Novikov I. D., 1983, reas.book,